ôDynamical Characteristics of Drought in the Caribbean from Observations and Simulations *ô*

DIMITRIS A. HERRERA, a TOBY R. AULT, AND CARLOS M. CARRILLO

Department of Earth, and Atmospheric Sciences, Cornell University, Ithaca, New York

JOHN T. FASULLO

National Center for Atmospheric Research, Boulder, Colorado

XIAOLU LI, COLIN P. EVANS, MARC J. ALESSI, AND NATALIE M. MAHOWALD

Department of Earth, and Atmospheric Sciences, Cornell University, Ithaca, New York

(Manuscript received 14 February 2020, in final form 8 July 2020)

ABSTRACT

Climate models consistently project a significant drying in the Caribbean during climate change, and between 2013 and 2016 the region experienced the worst multiyear drought in the historical period. Although dynamical mechanisms have been proposed to explain drought in the Caribbean, the contributions from mass convergence and advection to precipitation minus evaporation (P-E) anomalies during drought are unknown. Here we analyze the dynamics of contemporaneous droughts in the Caribbean by decomposing the contributions of mass convergence and advection to P-E using observational and simulated data. We find that droughts arise from an anomalous subsidence over the southeastern Caribbean and northeastern South America. Although the contributions from mass convergence and advection vary across the region, it is mass convergence that is the main driver of drought in our study area. A similar dynamical pattern is observed in simulated droughts using the Community Earth System Model (CESM) Large Ensemble (LENS).

1. Introduction

The Caribbean Islands and Central America are prone to relatively short, intense droughts that often cause losses in agriculture, municipal water shortages, and decreased hydropower generation (Larsen 2000; Méndez and Magaña 2010; Peters 2015; Herrera and Ault 2017; Hernández Ayala and Heslar 2019). During the unusually prolonged "Pan-Caribbean drought" of

Openotes content that is immediately available upon publication as open access.

Corresponding author: Dimitris A. Herrera, dah386@cornell.edu

2013–16 (Herrera et al. 2018), more than 3 million people were directly affected by food insecurity due to the failure of staple crops production (FAO 2016; OCHA 2015). Estimated losses from the Pan-Caribbean drought exceed hundreds of millions of dollars, primarily because of its effects on agriculture and tourism (FAO 2016; OCHA 2015). Similarly, droughts that occurred in 1997-98 and 2009-10 reduced crop yields from 20% to over 30%, leading to a significant increase in food prices across the Caribbean (Peters 2015; FAO 2016). In Trinidad and Tobago, for example, fruit prices increased by as much as 61% in 2010, partly due to the drought (Peters 2015; FAO 2016). These statistics suggest that slow-developing but persistent droughts can significantly affect the economies and food security of the Caribbean Islands and Central America. In fact, previous studies have identified the Caribbean Islands as one of the most vulnerable regions to climate change in the world, in part because of the projected drying in the coming decades (IPCC 2014; Karnauskas et al. 2016, 2018).

DOI: 10.1175/JCLI-D-20-0100.1

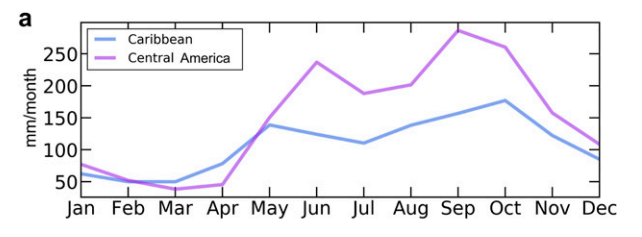
[©] Supplemental information related to this paper is available at the Journals Online website: https://doi.org/10.1175/JCLI-D-20-0100.s1.

^a Current affiliation: Universidad Autónoma de Santo Domingo, Santo Domingo, Dominican Republic.

Because of their tropical setting, the climatology of the Caribbean and Central America is characterized by a relatively small seasonal change in temperature, but a pronounced variation in precipitation (Magaña et al. 1999). In both regions, the annual cycle of precipitation follows a bimodal pattern characterized by two maxima in May-June and September-October, and a minimum in December-April (Fig. 1a) (Magaña et al. 1999; Gamble and Curtis 2008; Taylor et al. 2002). In the Caribbean, this pattern is consistent with the observed annual cycle of moisture convergence, which in turn is primarily sourced from the eastern Pacific and Atlantic intertropical convergence zone (ITCZ), and the western flank of the North Atlantic subtropical high (NASH) (Martinez et al. 2019). In contrast, the main sources of moisture in Central America are the Caribbean Sea and the eastern tropical Pacific Ocean, from where moisture is mainly carried by the Caribbean low-level jet (CLLJ) and the Choco jet (CJ), respectively (Durán-Quesada et al. 2017).

During the wet season (May-October), a relatively dry period occurs between July and August known as the "midsummer drought" (MSD) (Magaña et al. 1999; Gamble and Curtis 2008) (Fig. 1a). The dynamics underpinning the MSD are not well understood, but they likely involve a different mechanism for the Caribbean and Central America (Magaña et al. 1999; Gamble and Curtis 2008). For example, Giannini et al. (2001a,b) and Gamble and Curtis (2008) have proposed that the expansion of the North Atlantic subtropical high in July might play a critical role in the onset of the MSD in the Caribbean. According to this hypothesis, the intensification of NASH diminishes precipitation in this region by strengthening trade winds and by promoting vertical atmospheric stability (Gamble and Curtis 2008). In contrast, in Central America the MSD might be driven by the latitudinal migration of the ITCZ and changes in the low-level winds in the Pacific coast of Central America (Magaña et al. 1999). Regardless of the dynamical causes of the MSD, Caribbean droughts often unfold with an anomalously persistent MSD and subsequent failure of the September-October peak of the rainy season.

Some of the worst droughts in the Caribbean and Central America have occurred during El Niño events (Peters 2015; Herrera and Ault 2017), and multiple studies have linked drought variability in these regions with El Niño–Southern Oscillation (ENSO) (e.g., Giannini et al. 2000, 2001a,b; Jury et al. 2007; Méndez and Magaña 2010; Peters 2015). However, as suggested by Torres-Valcárcel (2018), the impacts of ENSO on drought in the Caribbean are neither temporally nor spatially uniform. Drought in the Caribbean and Central America has been further associated with the North



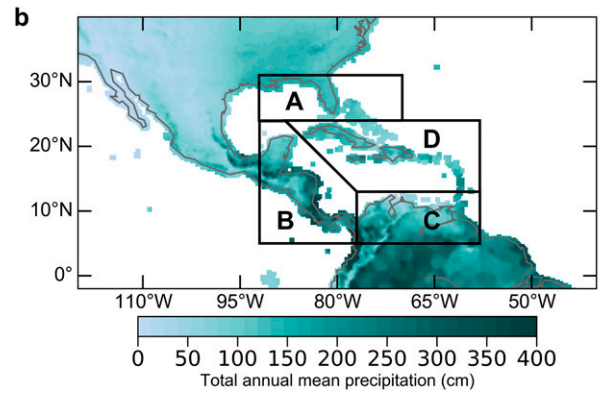


FIG. 1. Precipitation in the Caribbean and Central America: (a) Annual precipitation cycle for the Caribbean Islands and Central America from the Global Precipitation Climate Centre (GPCC), and (b) annual mean precipitation in our study domain (1950–2018), and the subregions we divide it into for this work: the Florida Peninsula (region A), Central America (region B), northern South America (region C), and the Caribbean (region D).

Atlantic Oscillation (NAO), the Madden–Julian oscillation (MJO), and the Atlantic multidecadal oscillation (AMO) (Enfield and Alfaro 1999; Giannini et al. 2000, 2001a,b; Taylor et al. 2002; Gamble and Curtis 2008; Martin and Schumacher 2011). The NAO impacts drought in both regions by changing the intensity of the NASH and the CLLJ (Giannini et al. 2000, 2001a,b; Taylor et al. 2002; Martin and Schumacher 2011).

Although there are some constraints on the dynamical causes of ENSO and NAO-driven droughts in the Caribbean and Central America (e.g., Rogers 1988; Giannini et al. 2000, 2001a,b; Taylor et al. 2002), the occurrence of drought in the absence of El Niño (e.g., Herrera and Ault 2017; Herrera et al. 2018) suggests that other dynamical and/or thermodynamical processes also modulate drought variability in these regions. Importantly, the pronounced topographical gradients of the Caribbean Islands and Central America might further influence drought variation at local scales through thermodynamical and dynamical processes (e.g., Durán-Quesada et al. 2017; Herrera and Ault 2017; Torres-Valcárcel 2018).

Global climate models consistently project an increase in aridity for the Caribbean and Central America as a result of anthropogenic climate change (e.g., Neelin

et al. 2006; Rauscher et al. 2008; Centella et al. 2008; Taylor et al. 2013; IPCC 2014). Previous studies have suggested that such a drying might be due to an earlier onset of the MSD and a stronger, longer-lasting, CLLJ (Rauscher et al. 2008; Taylor et al. 2013). Moisture budgets have been extensively used to diagnose the dynamical causes of extreme hydroclimate events, including droughts and flooding worldwide (e.g., Trenberth and Guillemot 1996; Seager and Henderson 2013; Seager et al. 2014). More recently, moisture budgets have been used to characterize the dynamical mechanisms of precipitation in the Caribbean and Central America (Durán-Quesada et al. 2017; Martinez et al. 2019). However, the relative contributions of mass converge and advection of moisture to drought have not yet been broadly implemented to investigate the dynamical causes of drought in the Caribbean Islands.

In this work, we provide further insights into the dynamical mechanisms of droughts that occurred in the Caribbean and Central America during the 1979– 2018 period using reanalysis and model simulations. Specifically, we aim to answer the following research questions in relation to the Caribbean Islands: 1) What are the physical processes associated with drought? 2) What are the relative contributions of mass convergence and advection of moisture to precipitation minus evaporation (P - E) anomalies during drought? 3) Are the dynamical causes of drought in climate models consistent with those from observations? To examine these questions, we use the European Centre for Medium-Range Weather Forecasts (ECMWF) interim reanalysis (ERA-Interim) (Dee et al. 2011) to calculate moisture budgets and moisture flux anomalies during three major droughts in the Caribbean: 1) 1997-98, 2) 2009-10, and 3) the 2013-16 Pan-Caribbean drought. These droughts are also analyzed in terms of global circulation and sea surface temperature (SST) anomalies, as many droughts in these regions have been linked to SST variations in the tropical Pacific and North Atlantic Oceans (Rogers 1988; Giannini et al. 2000, 2001a,b; Taylor et al. 2002; Gamble and Curtis 2008; Martin and Schumacher 2011; Herrera and Ault 2017). We further use the National Center for Atmospheric Research (NCAR) Community Earth System Model (CESM) Large Ensemble (LENS) (Kay et al. 2015) to assess the prevalent dynamical anomalies during drought in this model, which offers a larger sample size than the historical record alone.

2. Data and methods

a. Study area and climate data

As in Herrera and Ault (2017), our target area in this work is between 7°–33°N and 60°–90°W, which includes

the Caribbean Islands and Central America, and portions of South and North America (Fig. 1b). Given that drought variability differs from the subtropical Florida Peninsula to the tropical northern portion of South America (Amador 1998; Magaña et al. 1999; Gamble and Curtis 2008; Herrera and Ault 2017), we divide this area into four subregions to conduct our analysis (Fig. 1b). This division allows us to diagnose drought dynamics separately for the following regions: the Florida Peninsula (region A), Central America (region B), northern South America (region C), and the Caribbean (region D) (Fig. 1b).

1) ERA-INTERIM REANALYSIS

Table 1 provides a comprehensive list of the datasets used herein. To calculate the moisture budgets, we use the ERA-Interim reanalysis, which spans from January 1979 to August 2019 with temporal resolutions ranging from 3-hourly to monthly time steps, and $0.75^{\circ} \times 0.75^{\circ}$ horizontal resolution (Dee et al. 2011). It has a vertical resolution of 60 levels, with the top level at 0.1 hPa. ERA-Interim uses a four-dimensional variational assimilation scheme with an improved low-frequency variability, stratospheric circulation, and hydrological cycle (Dee et al. 2011). We use 6-hourly ERA-Interim data of surface pressure (P_s) , zonal (u) and meridional (v) components of the wind, and specific humidity (q) at $0.7^{\circ} \times 0.7^{\circ}$ Gaussian grid and 40 model levels for the 1979-2018 period. We further use horizontal wind and geopotential height (Z) also from ERA-Interim to assess the large-scale dynamic anomalies during the droughts studied, but at $1^{\circ} \times 1^{\circ}$ resolution.

Additionally, we use moisture budget data from NCAR's Climate and Global Dynamics Laboratory (CGD) to evaluate our moisture budget computations. This dataset is also calculated with ERA-Interim, but for the period 1979–2016 (Trenberth and Fasullo 2018; available at http:// www.cgd.ucar.edu/cas/catalog/reanalysis/ecmwf/erai/ index.html). Among other variables, this dataset provides monthly means of the vertically integrated moisture flux divergence, zonal and meridional moisture fluxes, and P-E (originally as E-P) at $0.5^{\circ} \times 0.5^{\circ}$ latitude/longitude resolution. As compared to moisture budgets directly calculated from ERA-Interim fields, the NCAR moisture budgets underwent a T-106 spectral truncation to reduce the "ringing" (i.e., spurious spatial patterns) of the budgets and were further corrected because mass convergence often does not match the surface pressure tendency (Trenberth 1991; Trenberth et al. 2011). This step is necessary to assess the long-term trends and variability of moisture transport, because the divergence estimated from reanalyses usually does not balance P - E (e.g., Trenberth et al. 2011; Seager and

TABLE 1. Observed climate datasets used in this work.

Variable	Dataset	Native resolution	Period used	Reference
Precipitation	GPCC ^a	1°	1979–2018	Schneider et al. (2015a,b)
•	$GPCP^b$	2°	1979-2018	Adler et al. 2003
Drought data	CarDrought ^c	4 km	1979-2019	Herrera and Ault (2017)
Sea surface temperature	ERSST v5 ^d	2°	1958-2018	Huang et al. (2017)
Specific humidity	ERA-Interim ^e	0.5°	1979-2018	Dee et al. (2011)
Zonal wind component	ERA-Interim	0.5°	1979-2018	Dee et al. (2011)
Meridional wind component	ERA-Interim	0.5°	1979-2018	Dee et al. (2011)
Surface pressure	ERA-Interim	0.5°	1979-2018	Dee et al. (2011)
Geopotential height	ERA-Interim	0.5°	1979-2018	Dee et al. (2011)
Surface pressure	ERA-Interim	0.5°	1979-2018	Dee et al. (2011)
Model data	CESM-LENS ^f	1°	1920-2006	Kay et al. 2015

^a GPCC: Global Precipitation Climatology Centre version 7.

Henderson 2013). However, in contrast to our moisture budget computations, CGD's dataset uses 28 model (σ) levels with the top of the atmosphere at $\sigma = 0.0$ and $\sigma = 1.0$ at the surface of the Earth, while we use 40σ levels of ERA-Interim.

2) OBSERVED GRIDDED-CLIMATE DATA

We use observed gridded products of monthly daily means of precipitation from the Global Precipitation Climatology Project (GPCP) (Adler et al. 2003) and monthly totals from the Global Precipitation Climatology Centre (GPCC) (Schneider et al. 2015a) (see Table S1 in the online supplemental material). We use SST data from NOAA's Extended Reconstructed Sea Surface Temperature version 5 (ERSSTv5) (Huang et al. 2017) to evaluate SST anomaly patterns associated with drought in the Caribbean and Central America. Although these products span different time intervals, we use them from January 1979 to December 2018 to be consistent with ERA-Interim.

The GPCP product combines rain gauge stations, satellite, and sounding observations to estimate monthly precipitation rates. This product spans from 1979 to near present, at 2.5° × 2.5° latitude/longitude (Adler et al. 2003). As compared to other observational gridded products, GPCP covers precipitation over land and over ocean, which is advantageous for the purpose of this work (e.g., to compare moisture transport with precipitation over ocean). We use the GPCP version 2.3 Combined Precipitation dataset, available at https://www.esrl.noaa.gov/psd/data/gridded/data.gpcp.html.

In addition to GPCP, we use the version 7 of GPCC (GPCC v7) to evaluate drought variation in the Caribbean and Central America across different gridded precipitation

products. GPCC totals monthly precipitation dataset uses 75 000 quality-controlled rain gauges worldwide (Schneider et al. 2015a) and approximately 400 stations in the Caribbean and Central America (Herrera and Ault 2017). GPCC has spatial resolutions from 0.5° to 2.5° latitude/longitude, and spans 1901–2013. However, the GPCC "combined product" (https://www.esrl.noaa.gov/psd/data/gridded/data.gpcc.html) that we use combines GPCC v7 with the GPCC v4 monitoring product spanning from 1901 to two months prior to present with 1° × 1° horizontal resolution (Schneider et al. 2015b).

ERSSTv5 is a global SST dataset spanning 1854 to near present at $2^{\circ} \times 2^{\circ}$ latitude/longitude. As compared to previous versions (e.g., ERSSTv3 and v4), ERSSTv5 uses more extensive input data, including the third version of the International Comprehensive Ocean–Atmosphere Dataset (ICOADS) (Huang et al. 2017). Further, this version has revised the bias correction, interpolation, and quality control procedures (Huang et al. 2017).

MODEL DATA

We use historical (i.e., 1920–2006) archives of 40 members from CESM-LENS (Kay et al. 2015) for two reasons: first, to assess the accuracy of this model in simulating drought dynamics in the Caribbean and Central America; and second, to increase the sample size to improve our understanding of the robust dynamics linked to drought. LENS is a 40-member ensemble of fully coupled simulations spanning 1920–2100, at approximately 1° horizontal resolution (Kay et al. 2015). It further includes two ~1000-yr-long preindustrial and control simulations, with the purpose of isolating

^b GPCP: Global Precipitation Climatology Project version 2.3.

^c CarDrought: Caribbean drought atlas.

^d ERSST v5: Extended Reconstructed Sea Surface Temperature version 5.

^e ERA-Interim: ECMWF interim reanalysis.

f CESM-LENS: Community Earth System Model's Large Ensemble.

anthropogenic climate change from internal variability (Kay et al. 2015). In contrast to what we do with ERA-Interim, these quantities are provided as direct model outputs. The details of how LENS compares with observational gridded products over the Caribbean are described in the online supplemental material (e.g., Figs. S1 and S2).

b. Methodology

We analyze the anomalies of moisture budgets and large-scale circulation, which are estimated as departures from the 1979–2018 climatology. The dynamics of following drought periods are evaluated in this work: 1) 1997–98, 2) 2009–10, and 3) 2013–16. Monthly moisture budgets and large-scale dynamics are analyzed at seasonal time scales to facilitate the interpretation of our findings. This is important because drought dynamics in the Caribbean and Central America have a different seasonal response to climate modes of variability such as ENSO (e.g., Giannini et al. 2000, 2001a,b; Jury et al. 2007; Herrera and Ault 2017). For example, the effects of El Niño on precipitation during the boreal summer (June-August) and the autumn (September-November) are the opposite from what is observed in early spring (March-May), with below normal precipitation in the summer and autumn, and positive anomalies in spring (Giannini et al. 2000, 2001a,b; Jury et al. 2007; Herrera and Ault 2017). We therefore analyze drought dynamics separately for March-May (MAM), June-August (JJA), September-November (SON), and December-February (DJF).

1) COMPUTATION OF MOISTURE BUDGETS

We calculate moisture budgets as in Seager and Henderson (2013) because this formulation allows us to separate the two components of moisture flux convergence: the part due to mass convergence and the part due to advection of moisture. Precipitation minus evaporation (P - E) can be thus diagnostically computed as

$$\begin{split} P - E &= -\frac{1}{g\rho w} \frac{\partial}{\partial t} \int_{0}^{P_{s}} q \Delta p - \frac{1}{g\rho w} \frac{\partial}{\partial t} \int_{0}^{P_{s}} (q\nabla \cdot \mathbf{v} + \mathbf{v} \cdot \nabla q) \, \Delta p \\ &- \frac{1}{g\rho w} q_{s} \mathbf{v}_{s} \cdot \nabla p_{s} \,, \end{split}$$

where g is the acceleration due to gravity, ρw is the density of water, the term $q\nabla \cdot \mathbf{v}$ is the mass convergence, and $\mathbf{v} \cdot \nabla q$ is the advection of moisture. The term $-(1/g\rho w)(\partial/\partial t)\int_0^{P_s} q\Delta p$ is the rate of change of the vertically integrated moisture or precipitable water tendency.

The boundary term $-(1/g\rho w)q_s \mathbf{v}_s \cdot \nabla p_s$ is therefore needed as a result of this approximation, but it is usually neglected (Seager and Henderson 2013). To account for the contribution of the mean flow and transient eddies to the total moisture convergence, Eq. (1) can be further expressed as

$$\overline{P} - \overline{E} = -\frac{1}{g\rho w} \left\{ \sum_{k=1}^{K} \left[(\overline{q_k} \nabla \cdot \overline{\mathbf{v}_k} + \overline{\mathbf{v}_k} \cdot \nabla \overline{q_k}) \overline{\Delta p} \right] + \nabla \cdot \sum_{k=1}^{K} \overline{\mathbf{v}'_{(6,k)} q'_{(6,k)}} \Delta p_k} \right\} - \overline{q_s \mathbf{v}_s} \cdot \overline{\nabla p_s}, \quad (2)$$

where the upper bar represents the total moisture flux for a specific month, and the primes are 6-hourly departures from the monthly mean flow. Notice that we ignore the precipitable water tendency, since this term is relatively small on monthly time steps as compared to the total moisture flux convergence.

Most atmospheric reanalyses do not conserve mass (e.g., Trenberth and Fasullo 2018). This may be due to, for example, the temporal and spatial heterogeneity of the assimilated observational climate data (Trenberth et al. 2011; Trenberth and Fasullo 2018). Efforts to circumvent this limitation focus on mass correction methods (e.g., Trenberth 1991; Trenberth et al. 1995; Trenberth and Fasullo 2018), usually based on barotropic, or "dry-air," corrections. To improve the accuracy of our analysis, we therefore mass-correct moisture transport and moisture flux convergence computations, as in Trenberth (1991) and Trenberth and Fasullo (2018). This approach involves two steps: first, a barotropic mass correction of wind velocities **v** is applied such that

$$R = \left(\frac{\partial P_s}{\partial t} - g \frac{\partial w}{\partial t}\right) + \nabla \cdot \int_0^{P_s} (1 - q) \mathbf{v}^* dp, \qquad (3)$$

where R is the mass budget residual and v^* is the non-corrected velocity field. Associated with R, a function χ is defined as

$$\chi = \nabla^{-2}R,\tag{4}$$

and thus

(1)

$$\mathbf{v}^{c1} = \nabla_{_{\boldsymbol{\chi}}}/(p_{_{\boldsymbol{S}}} - p_{_{\boldsymbol{t}}} - gw), \tag{5}$$

where the term \mathbf{v}^{c1} is the mass-corrected winds. The second step includes a mass correction to account for the mass of precipitated moisture. To do so, we separate moisture transport into its rotational $(\mathbf{v}q^r)$ and divergent $(\mathbf{v}q^d)$ components as

$$\mathbf{v}q = (\mathbf{v}q^r) + (\mathbf{v}q^d). \tag{6}$$

We then set $\mathbf{v}^{c2} = (\mathbf{v}q^d)$, and thus, the mass-corrected wind velocities \mathbf{v} are defined as

$$\mathbf{v} = \mathbf{v}^{c1} - \mathbf{v}^{c2} \,. \tag{7}$$

Also, since the term $-(1/g\rho w)\int_0^{P_s} (q\nabla \cdot \mathbf{v} + \mathbf{v} \cdot \nabla q)\Delta p - (1/g\rho w)q_s\mathbf{v}_s \cdot \nabla p_s$ is equal to $\nabla \cdot (1/g)\int_0^{P_s} qv \, dp$, we correct mass convergence and advection of moisture gradients separately as

$$MC_{corr} \approx -\frac{1}{g\rho w} \int_{0}^{P_{s}} [(q\nabla \cdot \mathbf{v}) \, \Delta p] - \frac{\nabla \cdot \frac{1}{g} \int_{0}^{P_{s}} q\mathbf{v} \, dp}{2}, \quad (8)$$

$$ADVQ_{corr} \approx -\frac{1}{g\rho w} \int_{0}^{P_{s}} (\mathbf{v} \cdot \nabla q) \, \Delta p - \frac{\nabla \cdot \frac{1}{g} \int_{0}^{P_{s}} q\mathbf{v} \, dp}{2}, \quad (9)$$

where the terms MC_{corr} and $ADVQ_{corr}$ are the mass-corrected mass convergence and advection of moisture, respectively.

2) OBSERVED LARGE-SCALE DYNAMICS ANALYSIS

Large-scale patterns of NASH, CLLJ, and global circulation are analyzed by compositing monthly SST, geopotential height, and horizontal wind anomalies of the observed droughts. The resulting patterns are then assessed for consistency with moisture flux anomalies from ERA-Interim. Geopotential height anomalies are detrended to remove the effects of the warming trend on atmospheric expansion during the period analyzed (e.g., Williams et al. 2017).

3) LONG-TERM TRENDS AND VARIABILITY IN OBSERVED MOISTURE BUDGETS

We calculate long-term (1979–2018) trends and variability of 1) P-E, 2) mass convergence, 3) advection of moisture gradients, and 4) moisture transport for each grid cell of our study area. Analyzing long-term trends in mass convergence and moisture advection separately provides further insight into the dynamical drivers of the drying observed in the Caribbean and Central America during the last 50 years (e.g., Herrera and Ault 2017). Trends are evaluated using two-tailed test, where trends with p values higher or equal to 0.05 at the 95% confidence interval are considered nonsignificant.

4) ASSESSMENT OF DROUGHT DYNAMICS IN LENS

Droughts in LENS are identified using model outputs of soil moisture and precipitation. Then, moisture budgets are calculated during simulated droughts in the Caribbean and Central America. To do so, we first regionally average soil moisture and precipitation and calculate their anomalies, as departures from the 1920–2006 climatology, over the Caribbean Islands. Monthly anomalies are then averaged to seasonal means for each year, and we normalize seasonal precipitation and soil moisture anomalies by calculating their *z* scores:

$$z = \frac{x - \overline{x}}{\sigma},\tag{10}$$

where z is the normalized variable, x is the variable seasonal mean for each year, \overline{x} is the long-term seasonal climatology, and σ is the standard deviation. We then select the droughts with $z \le -1$ from the normalized soil moisture and precipitation anomaly time series. Finally, we composite all seasons to obtain the seasonal climatology of simulated droughts. We repeated this procedure for each of the 40 members of LENS.

With the droughts identified from soil moisture and precipitation anomalies as a reference, we calculate P-Edirectly using model outputs of precipitation and evaporation, while moisture flux anomalies are calculated using specific humidity (q), surface pressure (P_0) , and wind vectors (v, u) as we do with ERA-Interim. Mass convergence and advection of moisture are calculated as $-(1/g\rho w)\left\{\sum_{k=1}^K \left[(\overline{q_k}\nabla\cdot\overline{\mathbf{v}_k})\overline{\Delta p}\right]\right\}$ and $-(1/g\rho w)\Big\{\sum_{k=1}^K[(\overline{\mathbf{v}_k}\nabla\cdot\overline{q_k})\,\overline{\Delta p}]\Big\}$, respectively. The consistency of LENS in simulating drought dynamics in the Caribbean and Central America is assessed from three perspectives: 1) comparing the seasonal long-term climatologies of P - E and moisture fluxes against the same climatologies from ERA-Interim, 2) analyzing the anomalies in P - E and moisture fluxes during simulated droughts, and 3) identifying NASH and CLLJ.

3. Results

a. Climatology of the vertically integrated moisture transport

The seasonal climatology of the vertically integrated moisture transports in the Caribbean and Central America is strongly dominated by changes in the low-level easterly fluxes (mostly represented by the CLLJ), the meridional migration of the ITCZ, and changes in the position and strength of NASH (Figs. 2 and 3). Although the ITCZ plays a major role in precipitation seasonality in Central America, regional and local features such as moisture transport from the Caribbean Sea and topography also contribute to local precipitation variability in this region, especially during the dry season. At regional scales in the Caribbean Islands, in contrast, the main source of moisture is from the North Atlantic carried by the trade

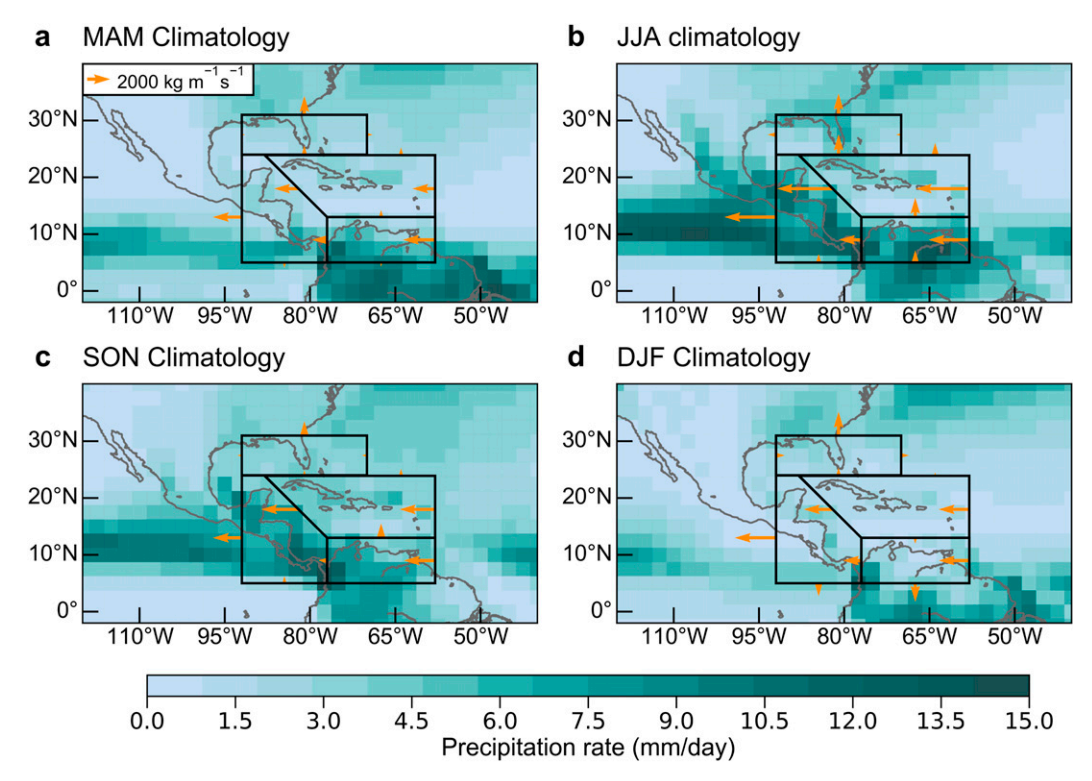


FIG. 2. Seasonal climatologies of precipitation (shaded) and vertically integrated moisture fluxes (vectors) in our study area. Precipitation seasonal climatology [from Global Precipitation Climatology Project (GPCP) 1979–2018] for (a) March–May, (b) June–August, (c) September–November, and (d) December–February. Arrows represent the total moisture flux across boundaries of the subregions studied in this work as in Fasullo and Webster (2002).

winds. The dry season for the Caribbean and Central America (from December to May or DJF and MAM) is characterized by dominant divergence over the Caribbean Sea. However, topography enhances convergence at very local scales. This is especially notable in Central America, where the Caribbean slope exhibits a relatively strong convergence in DJF, while the opposite is observed on the Pacific coast of Central America (Figs. 2 and 3). A similar feature is observed over the Caribbean Islands, although the magnitude is smaller than in Central America, probably due to the relatively low resolution of the ERA-Interim used here $(0.7^{\circ} \times 0.7^{\circ})$. The dry season is also dynamically characterized by a stronger CLLJ and the southwest expansion of NASH.

During the wet season in JJA and SON, there is an appreciable northward migration of the ITCZ accompanied by a relatively small shift in the CLLJ toward northern Central America (Figs. 2 and 3). This is noticeable with the increased moisture transport from the Caribbean Sea to Central America, with over $4 \times 10^3 \,\mathrm{kg}\,\mathrm{m}^{-1}\,\mathrm{s}^{-1}$. In the Caribbean Islands, this loss of moisture is compensated by an also increased moisture coming from the North Atlantic Ocean (Fig. 2). In the wet season, moisture fluxes are relatively large because

of the higher water vapor content of the atmosphere (due to warmer temperatures of the summer season and the northward migration of the ITCZ), but surface winds are slower than during the dry season (Fig. 2). In terms of convergence, there is a pronounced difference between JJA and SON. For example, in JJA there is persistent convergence in the western Caribbean (especially western Cuba), while in the eastern Caribbean Islands, consistent with the MSD, divergence is present (Fig. 3). In contrast, in SON convergence is observed throughout most of the Caribbean Islands.

b. Case studies of moisture budget anomalies from ERA-Interim

The 1997–98 drought begins in the spring (MAM) of 1997 and is characterized by anomalous moisture flux divergence in Central America and most of the Caribbean Islands (Figs. 4 and 5). The western portion of Cuba and northern Central America experienced above normal moisture convergence during this season, which is consistent with precipitation anomaly patterns commonly observed during El Niño events (e.g., Herrera and Ault 2017). In the summer (JJA) of 1997, the drought intensifies in southern Central America (e.g.,

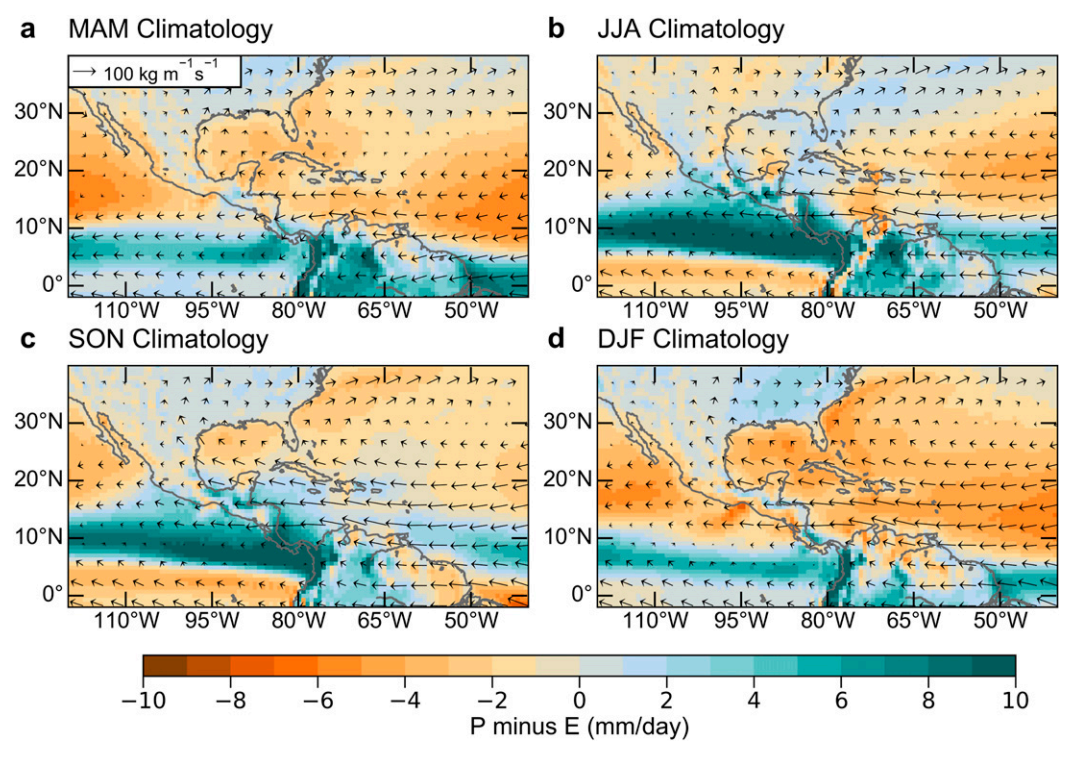


FIG. 3. Seasonal climatologies of precipitation minus evaporation (P - E; shaded) and vertically integrated moisture fluxes (arrows).

Panama and Costa Rica) as indicated by anomalous moisture flux divergence of up to $12 \,\mathrm{mm} \,\mathrm{day}^{-1}$ (Fig. 5). In the Caribbean Islands, drought conditions in JJA are similar to MAM except in Cuba. There, positive moisture convergence anomalies are present. In the autumn (SON), there is a noticeable change in moisture fluxes, especially in the eastern Pacific where fluxes changed from predominantly easterlies to westerlies of up to $6 \times 10^2 \,\mathrm{kg}\,\mathrm{m}^{-1}\,\mathrm{s}^{-1}$ above normal (Fig. 4). This anomalous moisture flux convergence is consistent with elevated El Niño SSTA in the eastern Pacific Ocean next to South America. In the winter of 1997-98 (DJF), drought conditions begin to diminish in most of the Caribbean Islands and small portions of Central America in association with anomalous moisture flux convergence over the Greater Antilles of Caribbean Islands and southeastern North America.

The drought of 2009–10 is one of the most severe recent droughts to occur in the Caribbean, but it mostly affected the Lesser Antilles and northern South America (Peters 2015; Herrera and Ault 2017). During this drought there is persistent moisture flux divergence over the Caribbean Sea beginning in MAM of 2009 through DJF 2009–10, with values ranging from 2 to 5 mm day⁻¹. Consistent with the rainfall deficits observed in weather stations in the Lesser Antilles (e.g., Peters 2015), the most intense moisture divergence and negative anomalies

in P-E are observed in the central/eastern Caribbean basin and northeastern South America. This picture contrasts with the average moisture convergence observed in Central America, with the exception of DJF in 2009–10 (Figs. 6 and 7). By the summer of 2010, the drought had subsided in most of the Caribbean and Central America with an average moisture convergence of \sim 5 mm day $^{-1}$.

As opposed to the previous droughts, the Pan-Caribbean drought of 2013-16 is characterized by spatial and temporal heterogeneity in terms of moisture flux convergence and divergence (Fig. 7). During this drought, two periods of persistent moisture divergence are observed in the Caribbean of a magnitude of ~ 3 and ~ 4 mm day⁻¹ on average, respectively. The first period spans from JJA to SON in 2014 and is characterized by having both moisture flux convergence and divergence in Central America. However, during this period there is an appreciable above normal moisture convergence in northern Central America (e.g., Yucatan Peninsula), which contrasts with the anomalous moisture divergence of the Caribbean. The second period occurs from MAM to SON in 2015 when the drought peaked and is similar to the one observed in 2014 (in terms of the spatial distribution of moisture convergence and divergence anomalies; Figs. 8 and 9). During both periods there is a strong moisture convergence anomaly, especially during JJA, in the

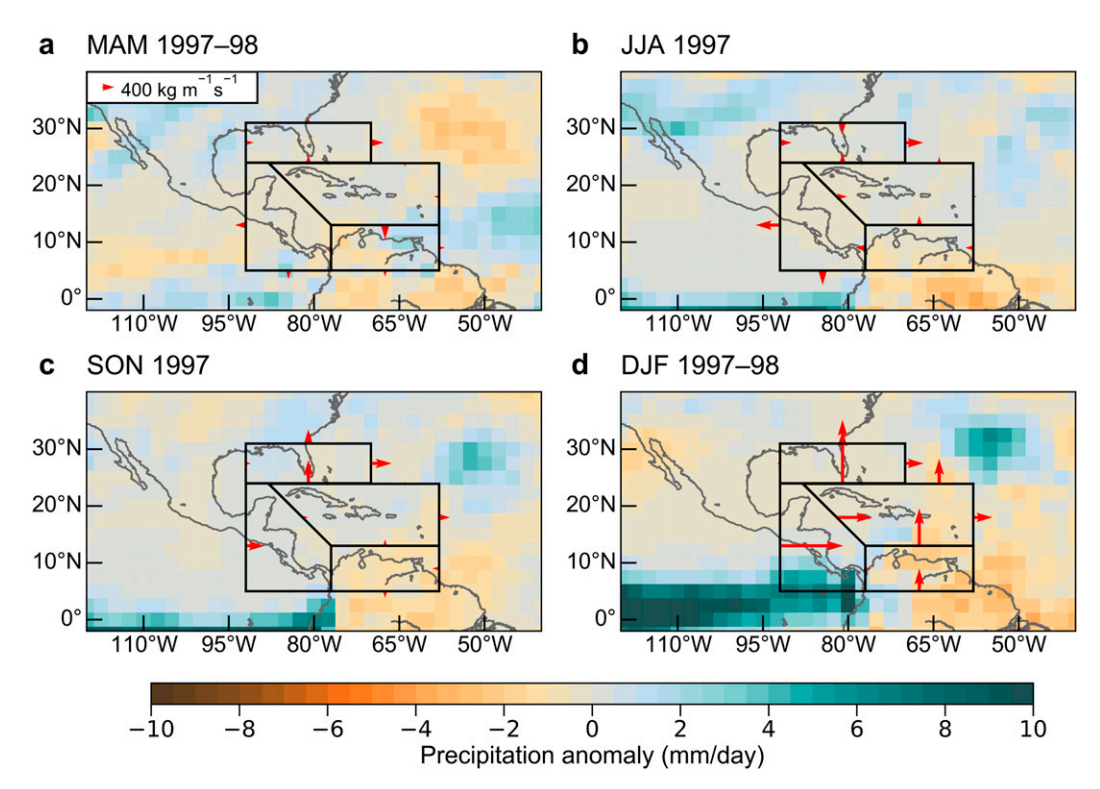


FIG. 4. Precipitation and moisture flux anomalies during the 1997–98 drought. Arrows represent total moisture flux anomalies across key boundaries.

eastern tropical Pacific near southern Central America, reaching more than 10 mm day⁻¹ (Fig. 9). This pattern is consistent with the strong El Niño of 2015 and the El Niño-like conditions in the summer of 2014. Beginning

in MAM 2016, however, the pattern is almost the opposite: a strong divergence anomaly (>12 mm day⁻¹) is observed next to southern Central America (Fig. 9), which is likely related to the onset of a weak La Niña

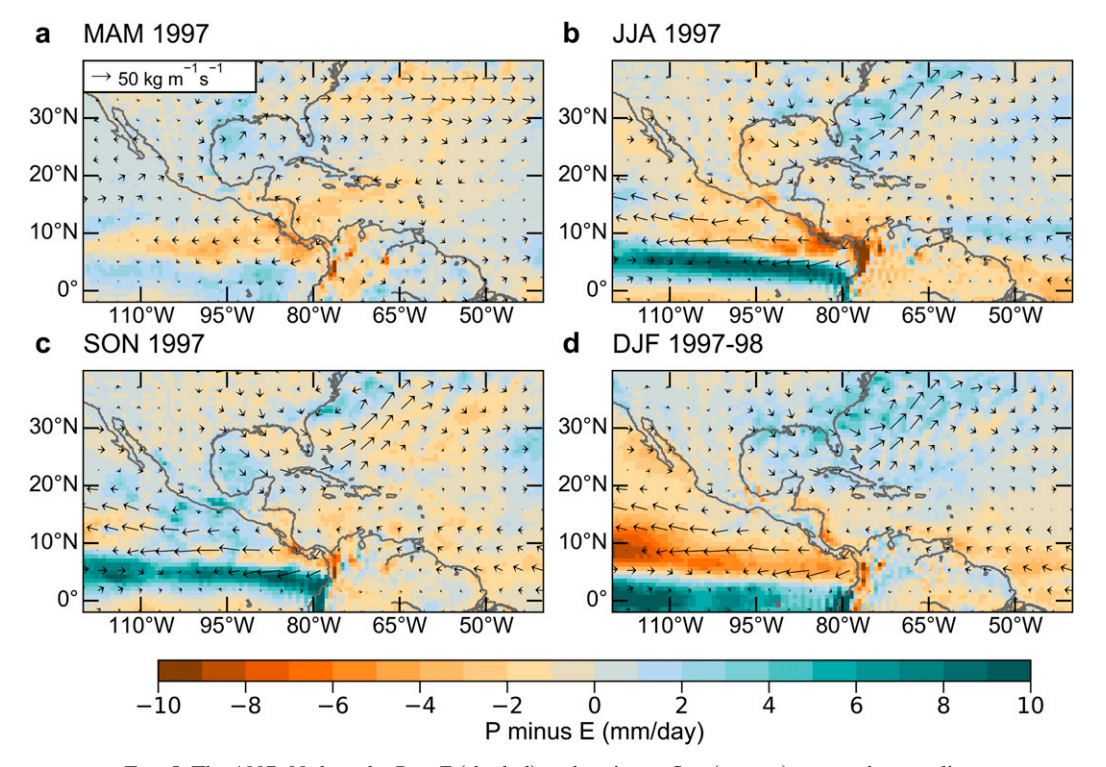


FIG. 5. The 1997–98 drought P-E (shaded) and moisture flux (arrows) seasonal anomalies.

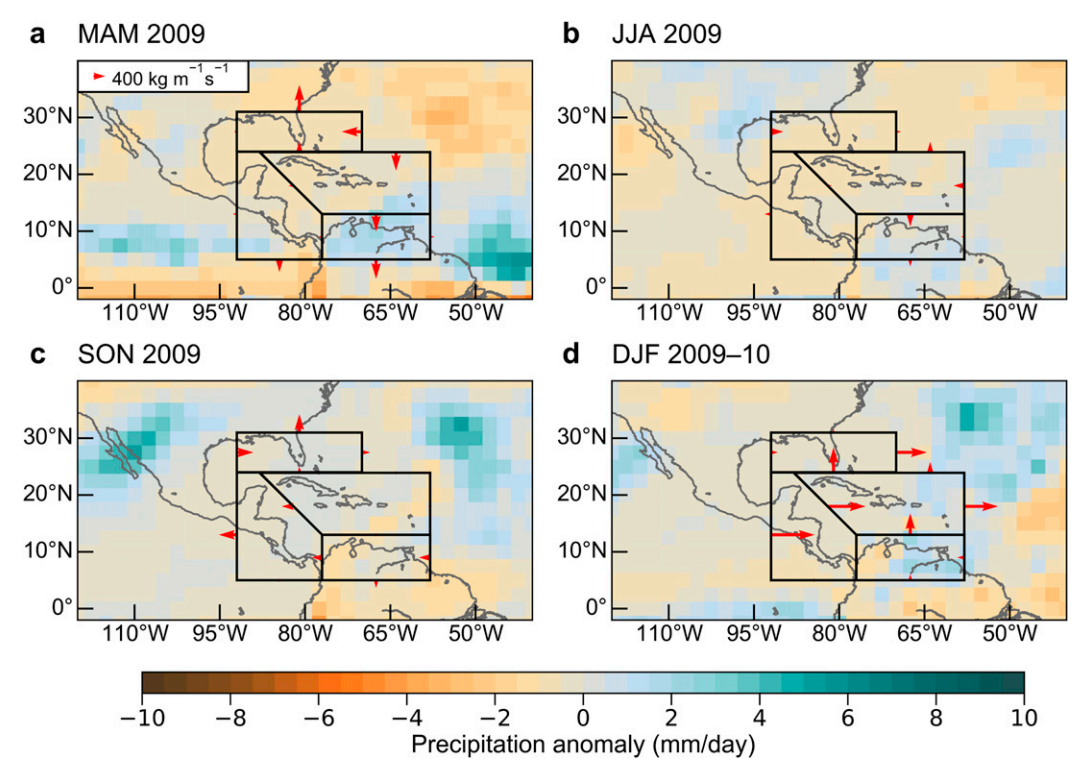


FIG. 6. As in Fig. 4, but for the 2009–10 drought in the Caribbean.

in 2016. In terms of moisture flux anomalies, this drought is characterized by increased loss of moisture of up to $-2\times 10^3\,{\rm kg\,m^{-1}\,s^{-1}}$ along the western boundaries of both the Caribbean Islands and Central America in MAM of 2014

and 2015, whereas this pattern persists over Central America during the boreal summer (JJA) (Fig. 8).

During the Pan-Caribbean drought, advection of moisture anomalies contributed to negative values of

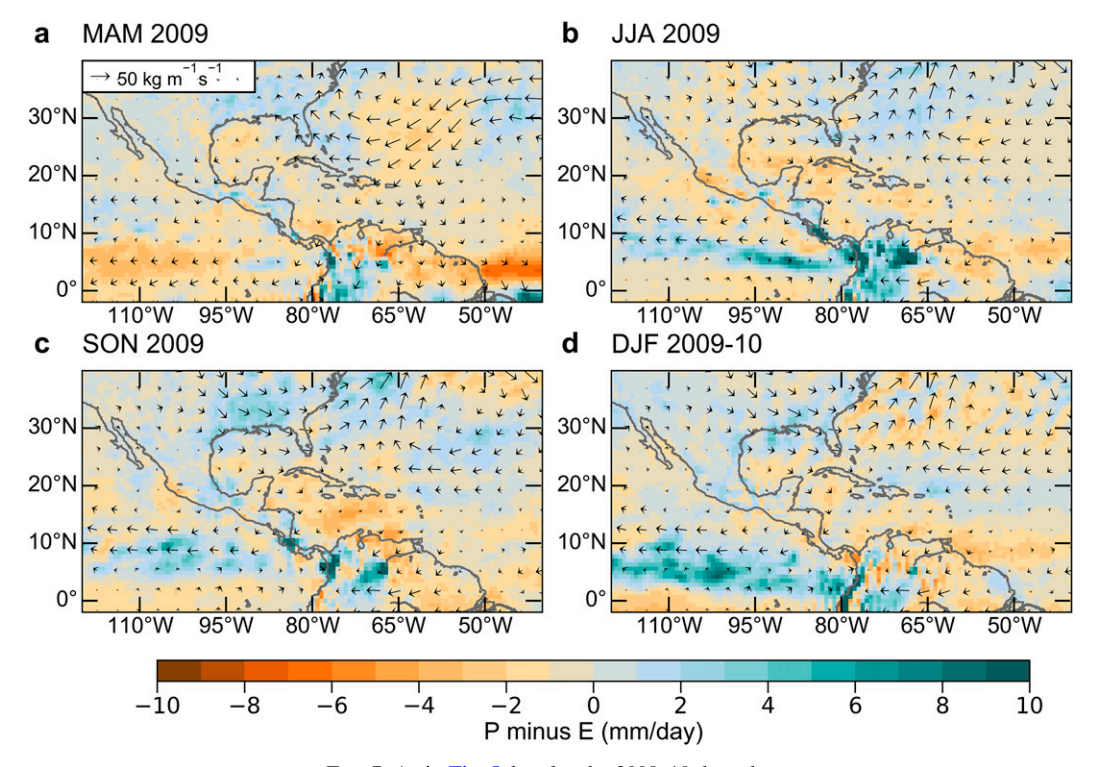


FIG. 7. As in Fig. 5, but for the 2009–10 drought.

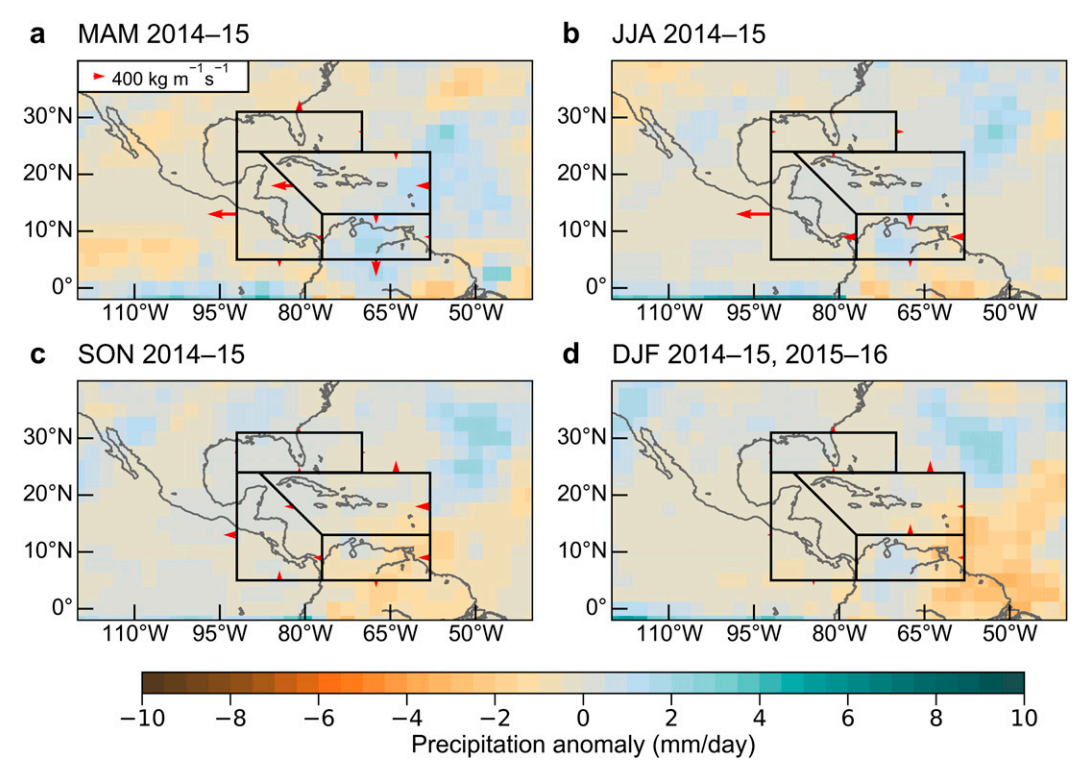


FIG. 8. As in Figs. 4 and 6, but for the 2013–16 Pan-Caribbean drought.

P - E (suggesting drying) of $-4 \,\mathrm{mm}\,\mathrm{day}^{-1}$ on average in Central America and northern South America in 2014 and 2015 (Fig. 10). In the Caribbean region, however, the advection of moisture contributed to a slight increase in moisture of $\sim 2 \,\mathrm{mm}\,\mathrm{day}^{-1}$, especially over the Greater Antilles, while the opposite is observed on the Lesser Antilles and over the Caribbean Sea during most seasons. However, the drying driven by the advection in Central America and northern South America is balanced by the wetting caused by mass convergence, with values of over 4 mm day⁻¹ but mostly over the Panama Isthmus (Fig. 11). This is also the opposite of what we observed over the Caribbean Islands, where mass convergence contributed to an average drying of $-4 \,\mathrm{mm}\,\mathrm{day}^{-1}$, although only in JJA. Notably, the spatial patterns in advection and mass convergence anomalies in JJA of 2014 and 2015 were remarkably similar, but anomalies in 2015 were more pronounced. The role of local topography in modulating local convergence is also noticeable (Figs. 10 and 11), especially when comparing the Caribbean and the Pacific coast of Central America.

c. Trends and variability of moisture budgets

Figure 12 shows the trends of P - E, mass convergence, and advection of moisture gradients for each of the subregions studied in this work. It is notable the prominent contribution of mass convergence to P - E

for the Caribbean Islands, Central America, and northern South America, while the opposite is observed to the north, over the Florida Peninsula. Trends toward drying conditions are statistically significant for the Caribbean Islands (Table 2), with a change in P-E of $-0.26\,\mathrm{mm}$ decade⁻¹ (p<0.05). This is consistent with the drying observed in convergence ($-0.19\,\mathrm{mm}$ decade⁻¹; p<0.05) and advection of moisture ($-0.067\,\mathrm{mm}$ decade⁻¹; p<0.05) for this region. In contrast, trends for the Florida Peninsula and northern South America are not significant (Table 2). In Central America, even though a significant wetting trend is observed in mass convergence ($0.23\,\mathrm{mm}$ decade⁻¹; p<0.05), it is offset by the drying from advection of moisture gradients (-0.136; p<0.05) (Table 2).

d. Large-scale dynamics during droughts from observations

Next, we analyze the global atmospheric and oceanic circulation and precipitation anomalies associated with these droughts. Figure 13 shows geopotential height anomalies at 200 hPa during the 1997–98 drought. Positive geopotential height anomalies are observed from the autumn (SON) of 1997 through the spring (MAM) of 1998 in the Caribbean, Central America, and northern South America. However, negative geopotential anomalies are observed at approximately

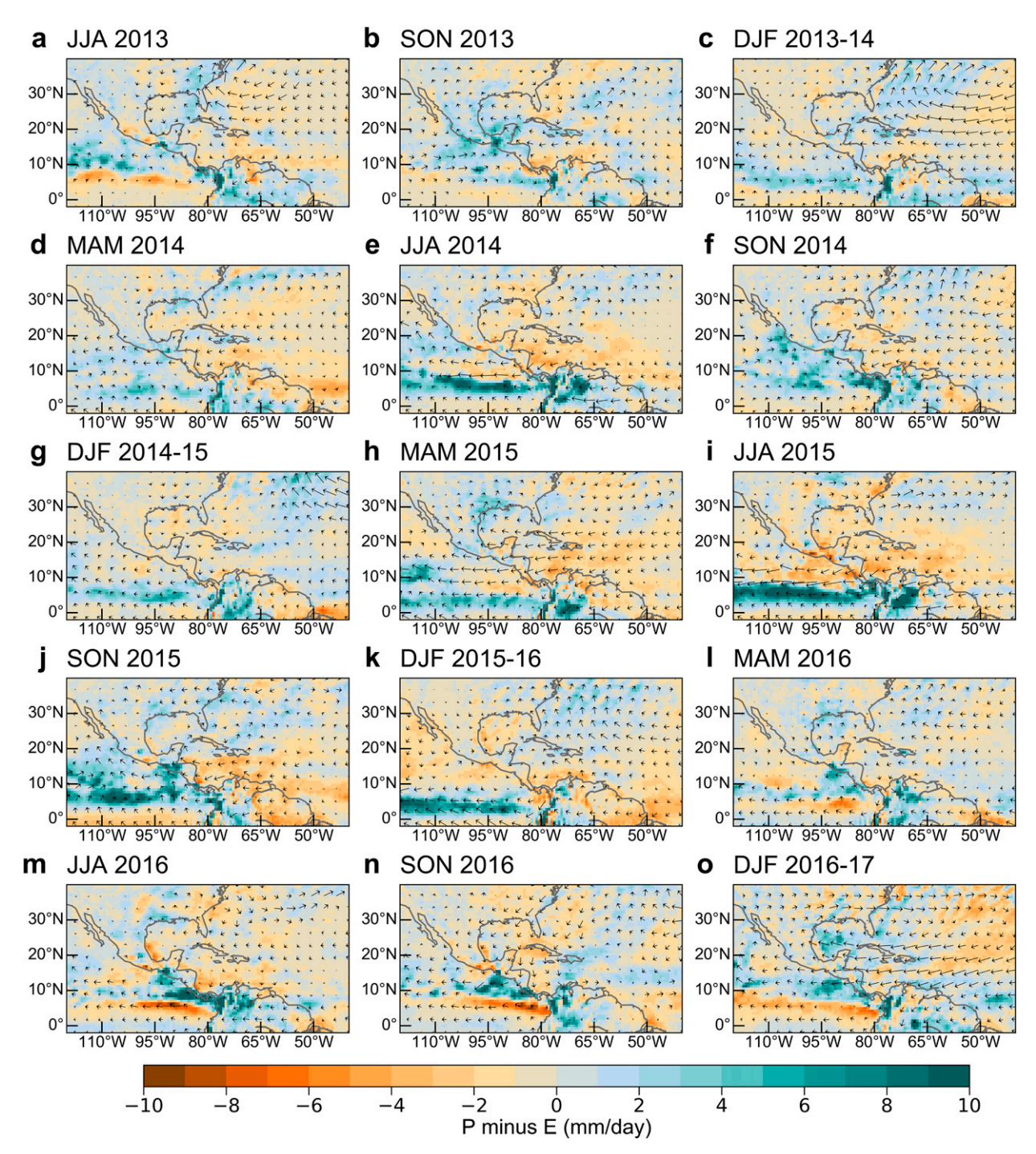


FIG. 9. As in Figs. 5 and 6, but during the Pan-Caribbean drought.

30°N (i.e., over the Florida Peninsula), separated by a narrow band of strong westerly wind anomalies. Geopotential and horizontal wind anomalies also indicate a persistent upper-level anticyclonic circulation during the drought over the central-eastern Caribbean Islands and Central America, which subsequently subsides

in the summer of 1998. These patterns are consistent with precipitation and SST anomalies observed during the drought (Fig. 13), which are characterized by a persistent dryness in Central America, the eastern Caribbean, and northern South America, and strong positive anomalies in the tropical Pacific associated with El Niño. This pattern in

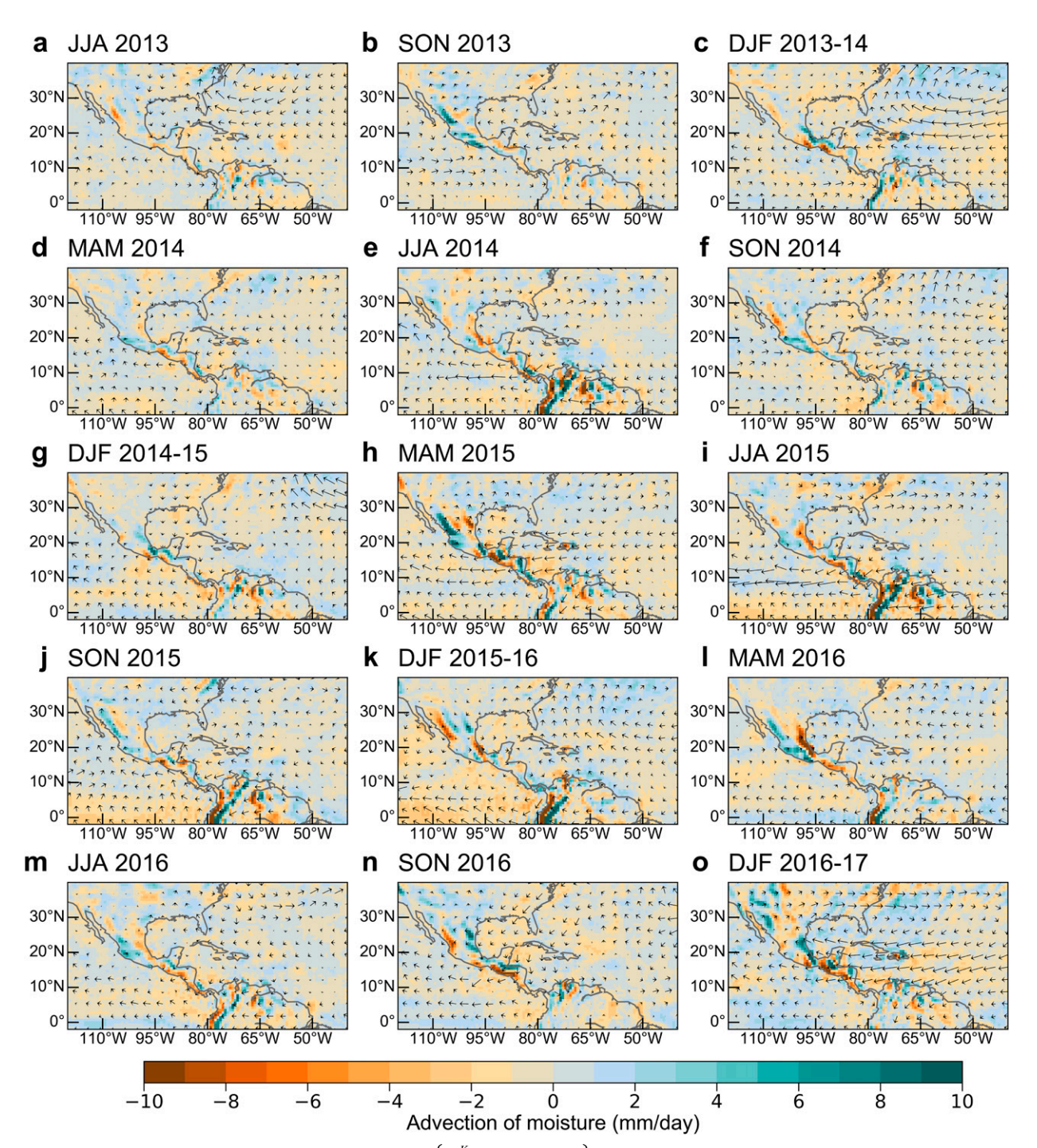


FIG. 10. Advection of moisture gradient, i.e., $-(1/g\rho w)\left\{\sum_{k=1}^{K}\left[(\overline{\mathbf{v}_{k}}\cdot\nabla\overline{q_{k}})\overline{\eta}\overline{\rho}\right]\right\}$, anomalies between MAM 2014 and JJA 2015. Advection of moisture contributed to a drying during these years of the Pan-Caribbean drought mostly in Central America and northern South America.

SST anomalies is commonly observed during El Niño (e.g., Giannini et al. 2000, 2001a,b; Herrera and Ault 2017).

Similarly, during the 2009–10 drought an anomalous upper-level anticyclonic circulation is present, mostly over the eastern Caribbean and northern South America

(Fig. 14). Although an El Niño event affected this region, this event is not as strong as the ones in 1997–98 and 2015–16. It is also characterized by the highest SST anomalies occurring in central-tropical Pacific (i.e., an El Niño "Modoki" event; e.g., Ashok et al. 2007). These findings

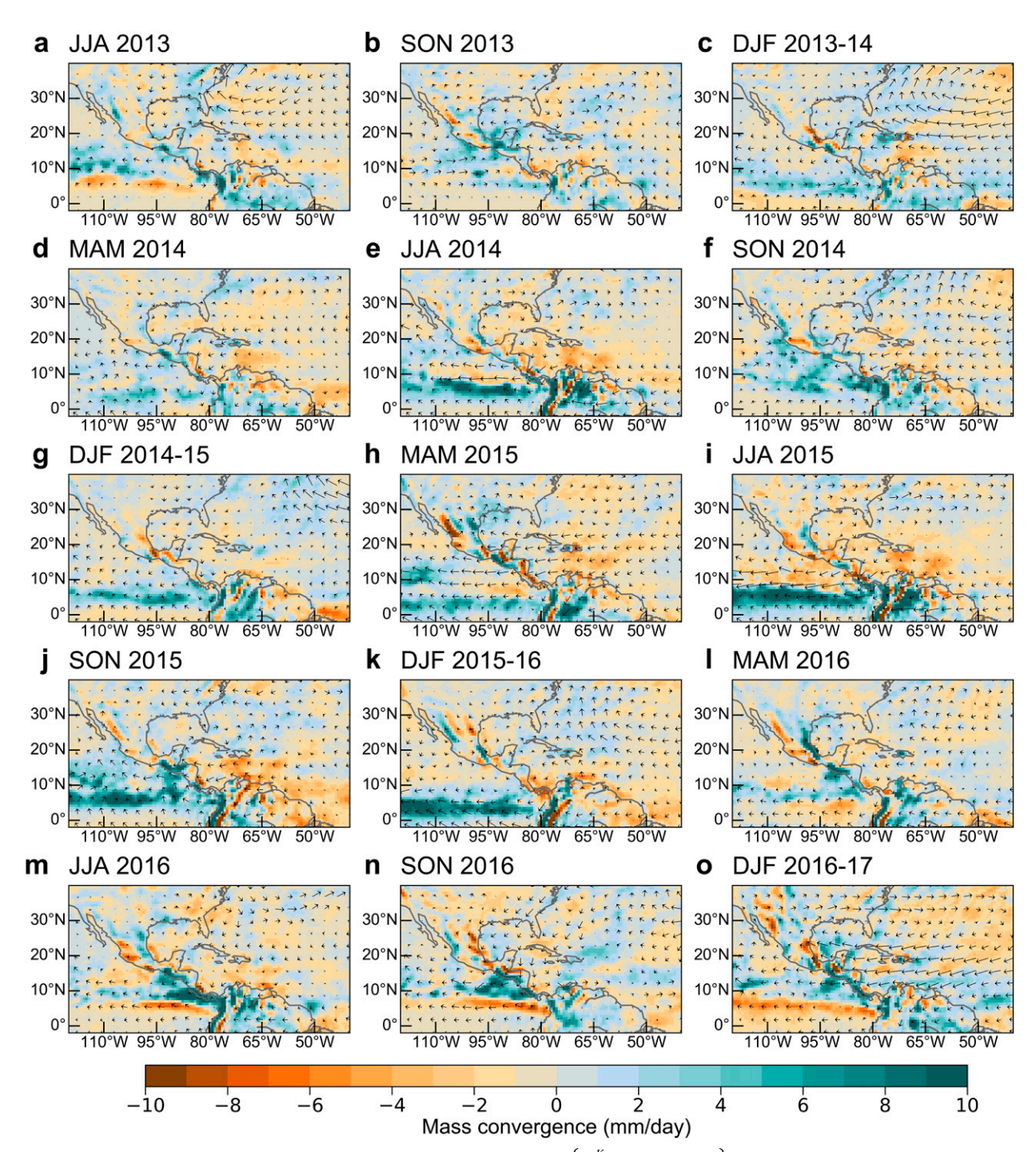


FIG. 11. As in Fig. 10, but for mass convergence anomalies, i.e., $-(1/g\rho w)\left\{\sum_{k=1}^{K}[(\overline{q_k}\nabla\cdot\overline{\mathbf{v}_k})\overline{\eta p}]\right\}$. As opposed to the moisture advection, mass convergence contributed to wetting the eastern equatorial Pacific and northern South America. In some cases, mass convergence offset the drying from the advection, especially over Panama and northwestern South America.

are consistent with the precipitation and SST anomalies observed between 2009 and 2010, where a warmer tropical Pacific and cooler tropical North Atlantic is associated with below-normal precipitation rates in the Lesser Antilles, northern South

America, and in parts of Central America and the Greater Antilles (Fig. 14).

The 2013–16 Pan-Caribbean drought is atypical in terms of its duration and severity (Herrera and Ault 2017; Herrera et al. 2018). Although between 2015 and

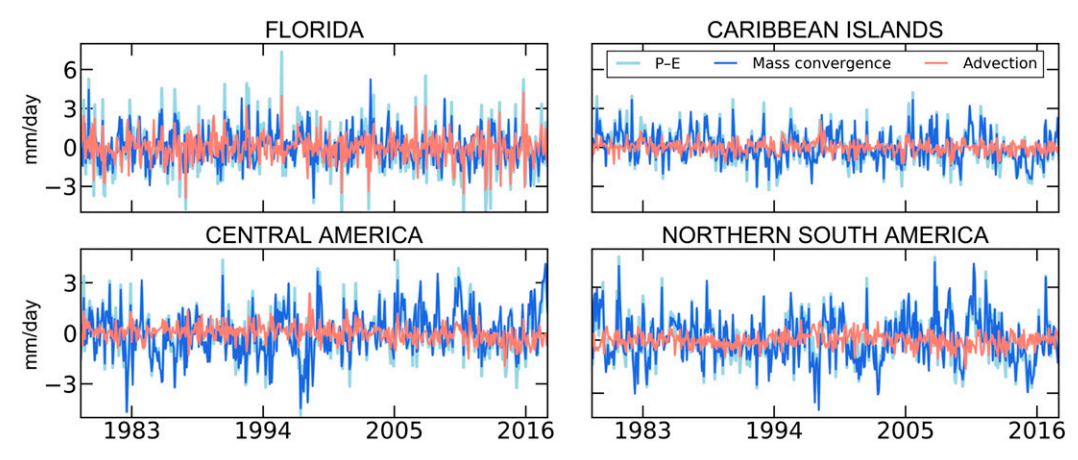


FIG. 12. Trends and variability of mean flow P - E, mass convergence, and advection of moisture gradients for each subregion analyzed in this work. It is notable the prominent contribution of mass convergence to P - E for the Caribbean Islands, Central America, and northern South America, as opposed to the Florida Peninsula.

2016 this drought is dynamically similar to previous droughts due to El Niño (Fig. 15), it unfolded in early 2013 in Central America and certain areas of the Caribbean. In 2013, significant anomalies in upper-level winds are not observed, while negative SST anomalies in the tropical Pacific and the Caribbean Sea are observed (Fig. 15). This pattern persists until the winter (DJF) of 2013, when the tropical Pacific begins to warm in the lead up to El Niño. In 2014, between JJA and DJF, an El Niño-like pattern is present (Fig. 15). A noticeable seesaw between the warmer tropical Pacific and colder tropical North Atlantic and Caribbean Sea is observed during this period. From MAM to DJF of 2015-16, a 200-hPa westerly wind anomaly is also observed over Central America and the Caribbean Sea, and a persistent anticyclonic circulation over the Caribbean Islands in SON of 2015 (Fig. 15). These observations are consistent with the below-normal precipitation registered in the Caribbean, Central America, and northern South America during almost all of 2015. In the summer of 2016, the drought begins to subside in the eastern Caribbean Islands and parts of Central America. Nevertheless, certain regions of Central America and western Caribbean are still under drought conditions, including portions of Hispaniola Island. The Caribbean Sea also warmed as drought subsided in the region. Between JJA and DJF 2016, colder SST anomalies over the tropical Pacific appears, consistent with the onset of a weak La Niña.

e. Moisture budget and large-scale anomalies from LENS

As shown in Figs. 16 and 17, the climatology of P - E, moisture fluxes, and precipitation from LENS is similar to that observed in ERA-Interim and GPCP. In general,

LENS captures the annual meridional migration of the ITCZ and the seasonal changes in the NASH and the CLLJ. However, there is a noticeable difference in the magnitude of total precipitation between LENS and GPCP, which is mostly pronounced over the tropical Pacific Ocean during JJA and SON (Fig. 16). These findings are consistent with the P-E climatologies, although LENS has a lower moisture convergence in MAM and DJF than ERA-Interim (Fig. 17).

Seasonal composites of precipitation during drought are characterized by a pronounced positive anomaly over a narrow band in the tropical Pacific, and negative anomalies over the Caribbean, Central America, and northern South America during SON (Fig. 18). A similar pattern is also observed in JJA and DJF, although the magnitude is significantly lower than in SON. This pattern is further consistent with the anomalies in P - E, although these anomalies are considerably smaller than the ones observed in precipitation. In contrast to precipitation anomalies, the largest moisture convergence anomaly is observed during JJA and DJF rather than in SON (Fig. 19).

As we found in ERA-Interim, simulated advection of moisture anomalies contributed to slight negative values in P-E in southern Central America, ranging from -0.2 to -0.5 mm day⁻¹ on average, and a wetting over the Caribbean Islands of ~ 0.3 mm day⁻¹ (Fig. 20). Additionally,

TABLE 2. Trends (mm decade⁻¹) of mean flow moisture budgets. Bold trends are statistically significant at the 95% level.

Region	P - E	Mass convergence	Advection
Florida	-0.07	-0.061	-0.012
Central America	0.09	0.232	-0.136
Northern South America	-0.09	-0.091	-0.001
Caribbean Islands	-0.26	-0.19	-0.067

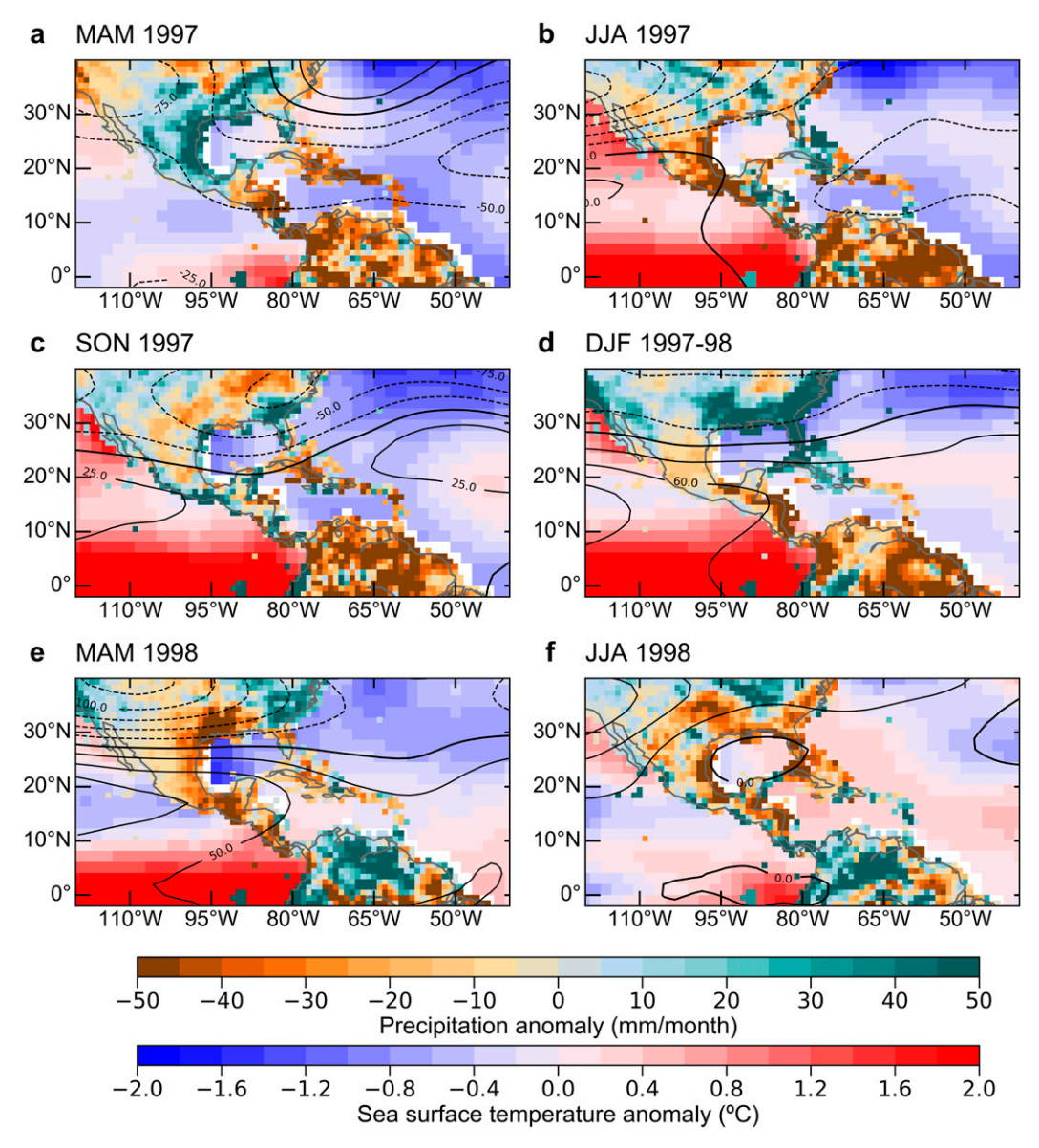


FIG. 13. Sea surface temperature (SST), precipitation, and geopotential height anomalies during the 1997–98 drought in the Caribbean and Central America. The characteristic positive SST anomalies over the eastern tropical Pacific was observed between the summer of 1997 (JJA) through the spring (MAM) of 1998.

and consistent with observations, mass convergence is associated with drought over the Caribbean and the northern portion of Central America in LENS, with anomalies of $-0.8 \,\mathrm{mm}\,\mathrm{day}^{-1}$ to P-E on average. This is particularly notable in DJF, when mass convergence contributed to drought almost over the entire domain (Fig. 21).

Anomalies in SST from LENS suggest that, during drought in the Caribbean, a warmer than normal tropical Pacific and a relatively cold SSTs occur in the North Atlantic during JJA, SON, and DJF (Fig. 22). The highest SST anomalies during drought in LENS are

observed in DJF over the tropical Pacific, whose geographic pattern is similar to that observed during El Niño events from instrumental records.

4. Discussion

a. Dynamical causes of the 1997–98, 2009–10, and 2013–16 droughts

Our findings suggest that the historical droughts studied here share some dynamical features in terms

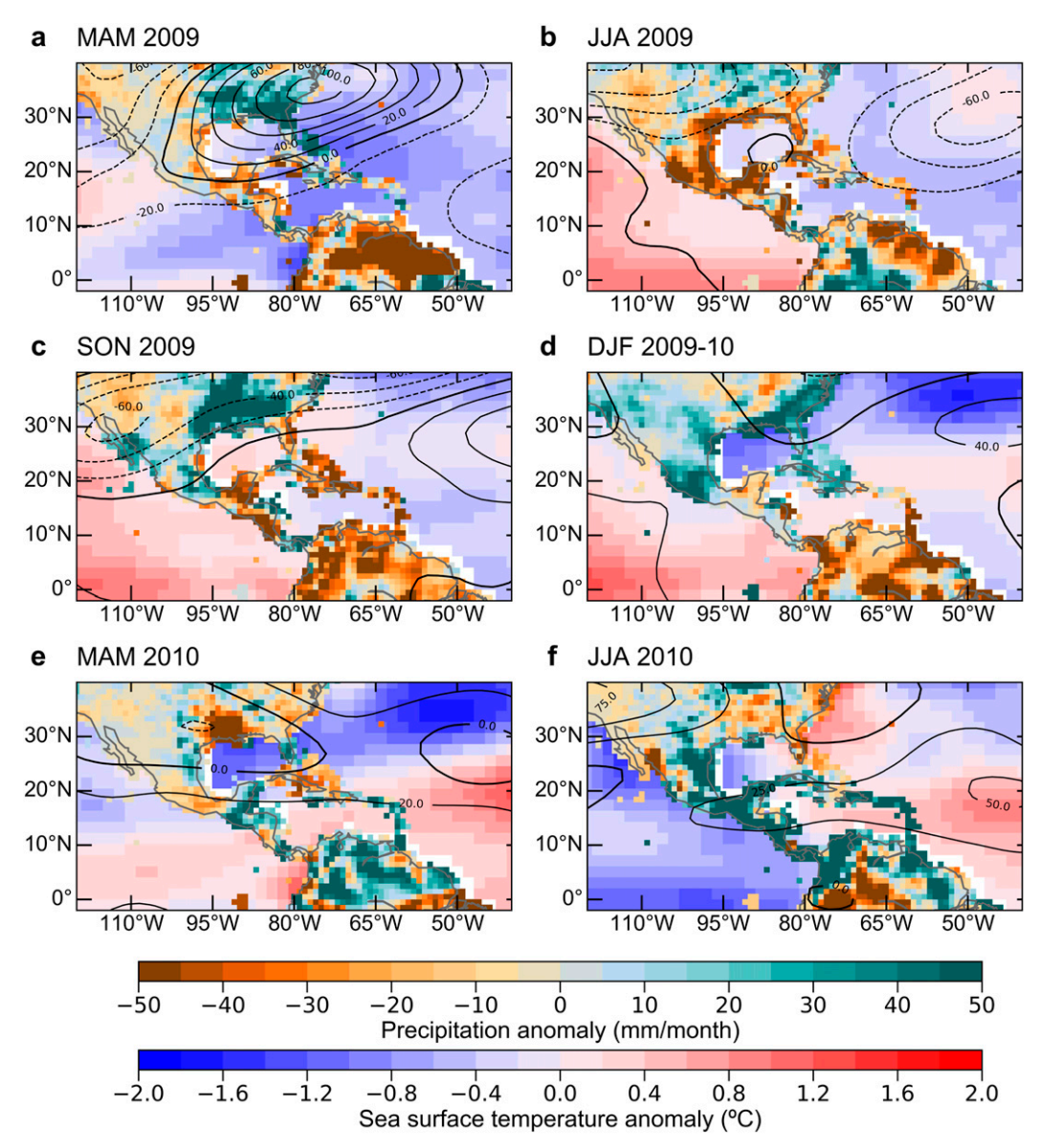


FIG. 14. As in Fig. 13, but for the 2009–10 drought.

of convergence and divergence of the vertically integrated moisture transport, P-E, SST, and precipitation anomaly patterns. During the three droughts we analyze, a persistent moisture divergence anomaly and decreased P-E are observed in most of the Caribbean basin, Central America, and northeastern South America (Figs. 4–9), suggestive of a subsiding air mass. These results are consistent with the reduced precipitation observed in GPCC. We also find that severe droughts in Central America, especially over the Caribbean coast, are associated with anomalously weak easterly winds represented by the CLLJ and/or a reduction of moisture coming from the eastern Pacific. This is noticeable, for example, in DJF of 1997–98,

MAM of 2009, JJA of 2014, and MAM, JJA, and SON of 2015. In contrast, in JJA of 2010, stronger easterly winds transporting moisture from the tropical North Atlantic are associated with increased precipitation in most of Central America and the Caribbean Islands (Figs. 6 and 7). Consistent with previous studies (e.g., Giannini et al. 2000, 2001a,b), SST anomalies are characterized by warmer than average SST over the tropical Pacific, and colder SSTs in the tropical North Atlantic and the Caribbean Sea (Figs. 13–15). This "tropical Pacific–tropical North Atlantic seesaw pattern" is a common feature observed during El Niño events (e.g., Giannini et al. 2000, 2001a,b; Enfield and Alfaro 1999). Since the droughts we analyze here

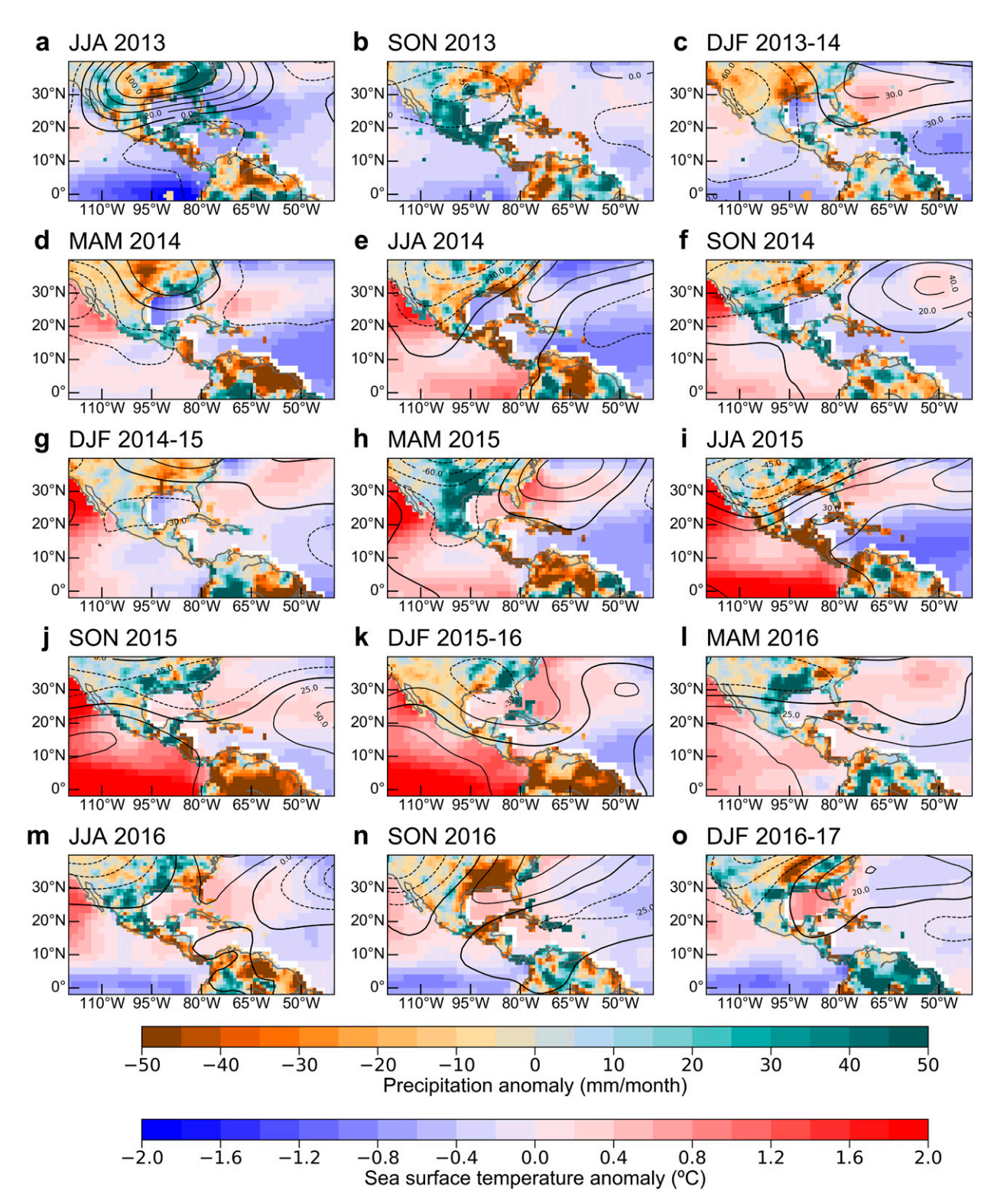


FIG. 15. As in Figs. 13 and 14, but during the 2013–16 Pan-Caribbean drought.

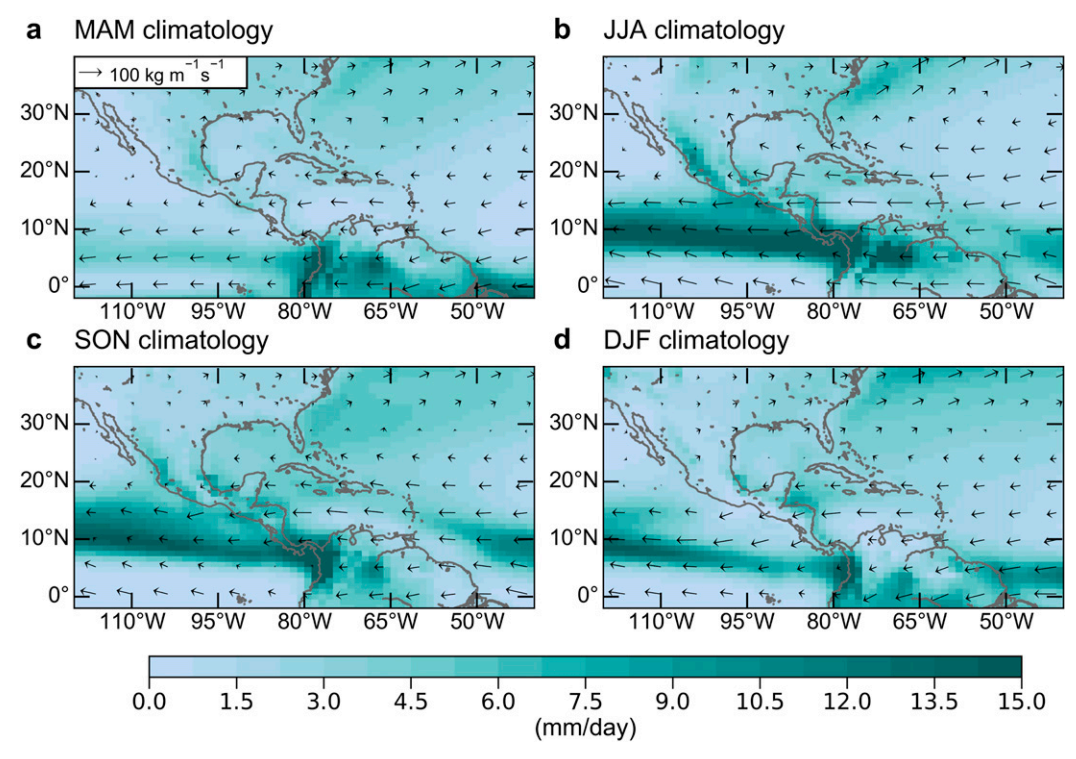


FIG. 16. Precipitation and moisture flux seasonal climatologies from LENS. The climatology is calculated from the full 1920–2006 interval.

occurred during El Niño, these SST anomaly patterns are expected.

The 2013–16 Pan-Caribbean drought also shares some dynamical characteristics of the previous droughts,

especially between JJA of 2014 and DJF of 2015–16 due to El Niño (Figs. 8 and 9). The major difference, however, is the duration, severity, and spatial extent, which affected over 80% of our study domain, particularly the

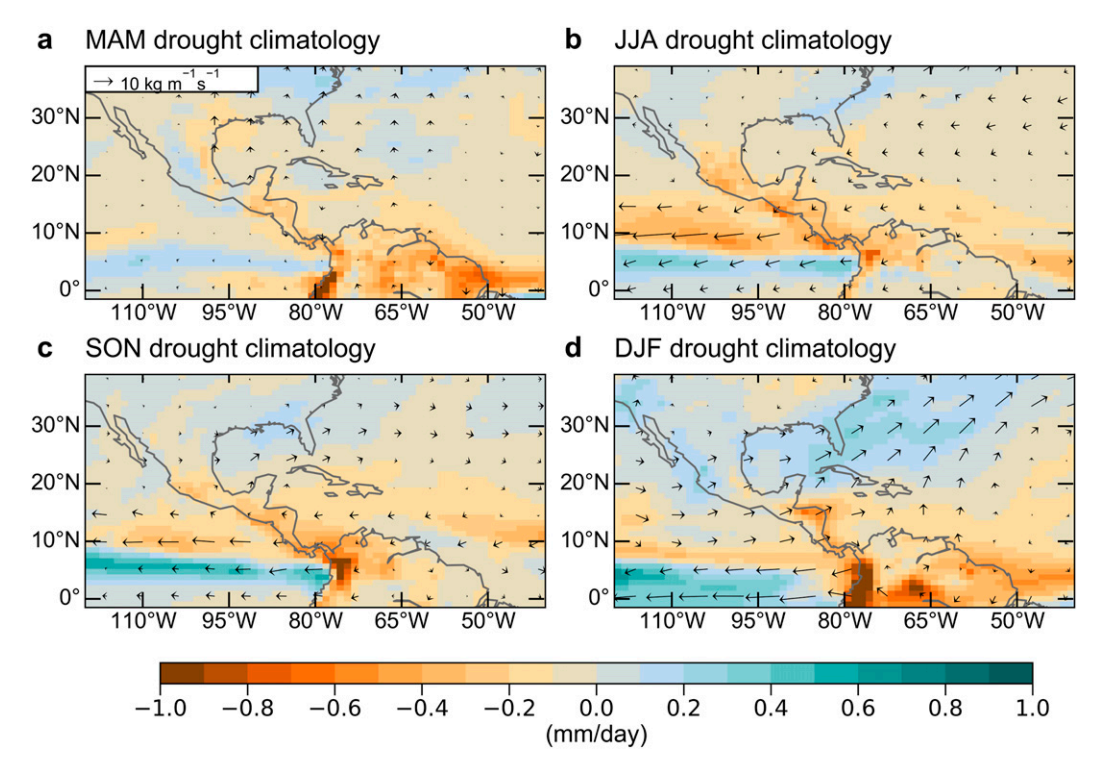


FIG. 17. As in Fig. 16, but for P - E.

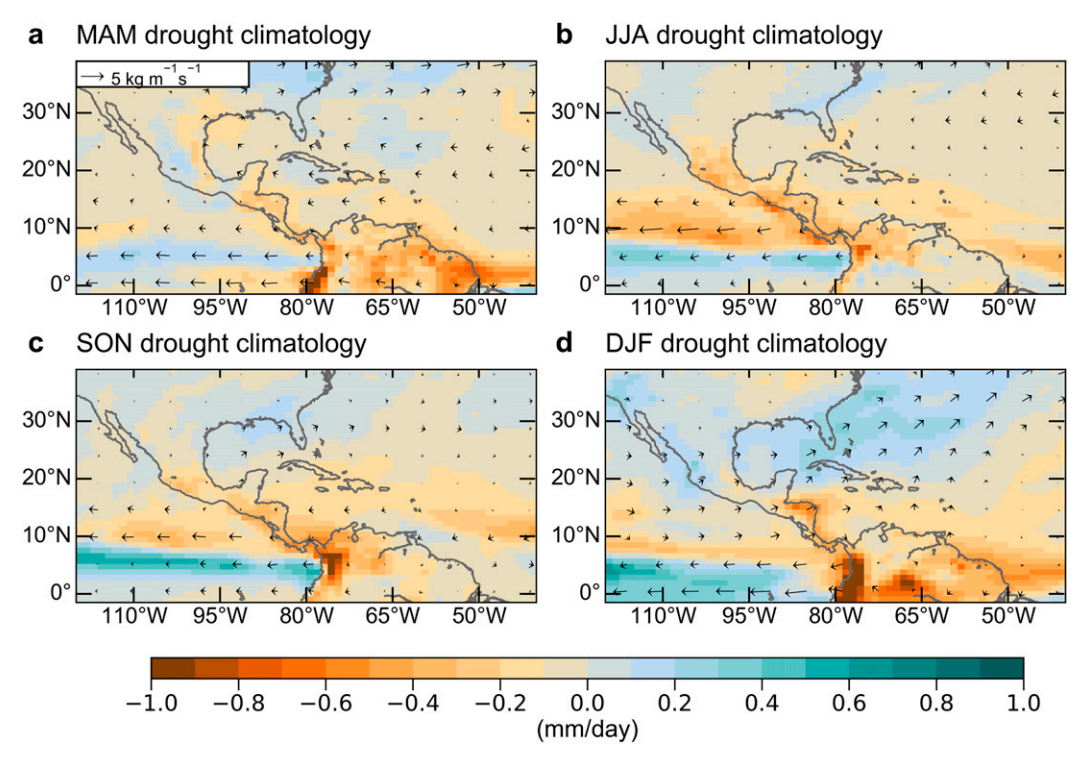


FIG. 18. Precipitation and moisture flux anomalies during drought in LENS. Each panel represents the long-term (1920–2006) seasonal climatology during drought from the 40 members used in this work. An El Niño-like pattern is observed during the seasons June-August (JJA) and September-November (SON).

Caribbean, northern South America, and Central America (Herrera and Ault 2017). As we suggest in Herrera et al. (2018), anthropogenic warming contributed to at least ~15%–17% of drought severity (as estimated using the self-calibrating Palmer Drought Severity Index) and ~7% of dry area over land in the Caribbean by increasing evapotranspiration rates. Dynamically, this drought is also different from previous El Niño droughts due to a longer-lasting El Niño-like pattern (Fig. 9). Although the 2015–16 event peaked in JJA of 2015, an El Niño-like SST anomaly pattern is present between JJA and SON of 2014 (Figs. 9 and 15). It is during the seasons of MAM-SON 2014 and MAM-DJF of 2015-16 when the highest moisture divergence anomalies are observed over the Caribbean and Central America. These patterns are consistent with the precipitation and upper-level wind anomalies observed during the Pan-Caribbean drought. Although during the Pan-Caribbean drought positive precipitation anomalies are observed (e.g., DJF 2014-15 and MAM-SON 2016), in many instances these higher precipitation rates are not enough to offset the soil drying of the previous seasons (Herrera and Ault 2017; Herrera et al. 2018).

During the Pan-Caribbean drought, the advection of moisture anomalies contributed to negative values in P − E across the Caribbean, Central America, and northern South America (Fig. 10). However, it is during JJA of 2014 and 2015 when moisture advection pushes these regions into a peak drying, especially over the Pacific coast of Central America, in a region known as the "dry corridor" (e.g., Anderson et al. 2019; Hidalgo et al. 2019). These findings are consistent with the moisture flux anomalies, which suggest a strong moisture advection (i.e., higher moisture flux anomalies driven by stronger horizontal winds) over these regions (Fig. 10).

In addition, mass convergence intensifies the drought between JJA of 2014 and 2015 over the Caribbean Islands, but it slightly contributes to wetting conditions during MAM, SON, and DJF (Fig. 11). It is noticeable that the strongest mass convergence anomaly observed over the equatorial eastern Pacific coincides with the highest mass divergence in the Caribbean Sea and northeastern South America, reminiscent of the seesaw pattern between both basins during El Niño-driven droughts in the Caribbean and Central America (e.g., Giannini et al. 2000, 2001a,b; Enfield and Alfaro 1999; Herrera and Ault 2017). This pattern is due to SST-driven changes in the Walker circulation; specifically, anomalous rising air over the equatorial eastern Pacific

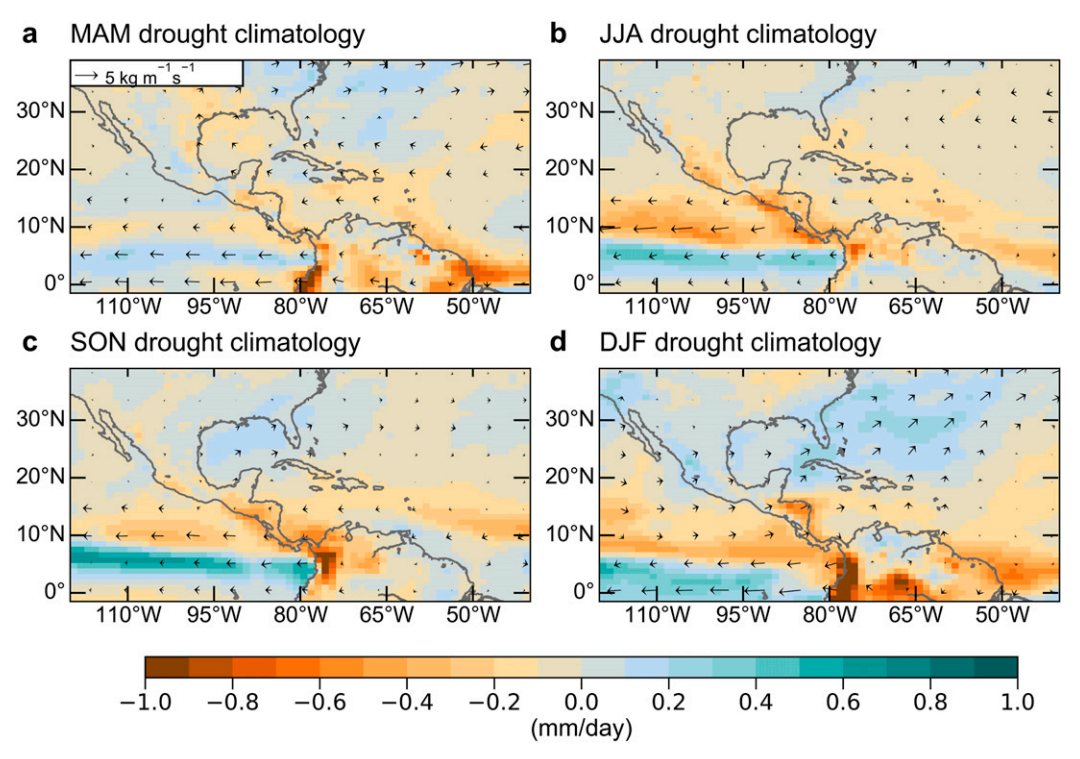


FIG. 19. As in Fig. 18, but for P - E in LENS.

and subsiding air over the Caribbean Sea, tropical North Atlantic, and northeastern South America. The strength of such an anomalous atmospheric circulation over our study domain depends on the SST anomaly gradient between the tropical Pacific and North Atlantic Oceans (e.g., Enfield and Alfaro 1999), where higher gradients are associated with a stronger atmospheric response. At the same time, according to Hidalgo et al. (2015), the teleconnection between the Caribbean Sea and tropical Pacific is related not only to changes in the Walker circulation, but also to local convection.

Because each El Niño event is different (i.e., ENSO diversity; Capotondi et al. 2015), the location of the anomalous mass convergence varies along with SST anomalies over the tropical Pacific. Subsequently, the position of the associated divergent flow, usually located over northeastern South America and the Caribbean Sea, also varies. This variation may, at least in part, explain why El Niño driven droughts in the Caribbean vary in terms of their severity and geographical extent (e.g., the 1997–98 versus the 2009–10 droughts).

Although the droughts analyzed in this work occurred during El Niño events, which may not represent other localized yet severe droughts across our study area, the resulting analysis suggests that mass convergence, rather than advection, is the main driver of drought. This is coherent with the dynamical mechanisms of El Niño—

driven droughts in our study domain previously explained, and is consistent with wetting observed in southeastern United States during drought in the Caribbean (e.g., Bishop et al. 2019).

b. Dynamical characteristics of drought in LENS

The moisture budgets from LENS also suggest a major influence of the tropical Pacific Ocean on drought severity across the Caribbean, Central America, and northern South America, as indicated by composites of SST anomalies co-occurring with drought (Fig. 22). The geographic patterns of these SST anomalies are comparable to those during El Niño events from observations. However, while the greatest negative anomalies in precipitation and P - E across our study area in LENS are observed in SON, the highest SST anomalies are found in DJF (e.g., Figs. 14-16), which differs from ERA-Interim where the greatest anomaly in rain is identified in JJA (e.g., Figs. 5-7). This discrepancy may be due to differences in the mean state precipitation between LENS and ERA-Interim over the study region. This may be also as a result of the computation of precipitation anomalies as the difference between the climatology and each month (rather than the ratio or percentage), which leads to higher precipitation anomalies during drought for SON in the wet season [\sim 386 mm yr⁻¹ (37%)], as compared to DJF in the dry season [$219 \,\mathrm{mm}\,\mathrm{yr}^{-1}$ (21%)].

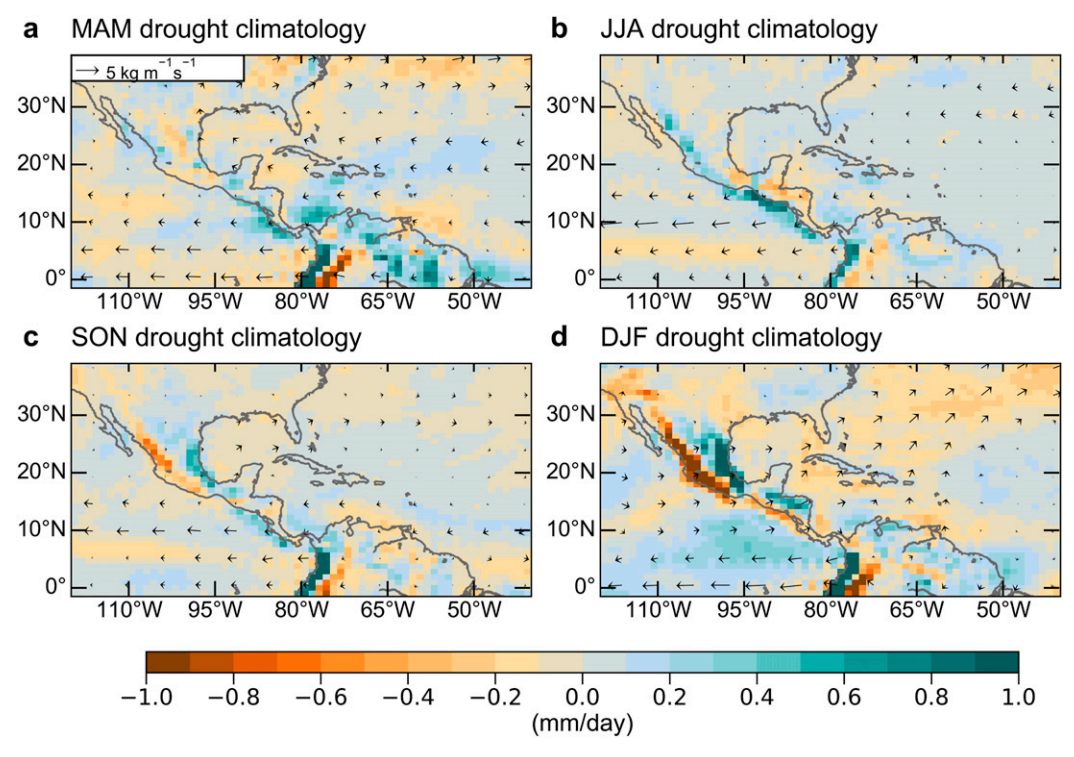


FIG. 20. Advection of moisture gradient anomalies from LENS. Consistent with observations, advection contributes to the drying over the eastern equatorial Pacific, just the north of the strong mass convergence associated with El Niño events.

Differences in the magnitude of precipitation and P-E anomalies between ERA-Interim and LENS arise for various reasons, such as comparing seasonal means during droughts occurring between 1920 and 2006 in the model against the dynamics of specific droughts in observations. In addition, we examine droughts in LENS using a 40-member ensemble, which also smooths out anomalies in precipitation and P-E. We further use outputs of precipitation and evaporation from LENS to calculate P-E, rather than diagnostically computing these terms with Eq. (1).

Because we use monthly outputs from LENS to calculate mass convergence and advection of moisture, the resulting computations are not as accurate as using daily or subdaily climate data (e.g., Seager and Henderson 2013). Regardless of this obvious limitation, we find that LENS adequately simulates the relative contributions of mass convergence and advection during drought, especially over Central America (Figs. 20 and 21). For example, LENS suggests mass convergence as the main driver in most of the study domain, especially over northeastern South America and the Caribbean Sea (Fig. 21). LENS is also consistent with the strong mass convergence over the eastern equatorial Pacific observed during El Niño events in ERA-Interim (e.g.,

Fig. 11). Consistent with observations, LENS indicates the mass divergence—and thus subsiding air—as the main cause of drought during most of the seasons of the year. As we previously mentioned, however, we should be cautious interpreting these results from LENS, given the limitations of our calculations and procedures using this model in this work. Future work should include subdaily data from LENS and evaluate the dynamics behind specific droughts in the model.

5. Conclusions

We assess the dynamical characteristics and atmospheric causes of three major droughts in the Caribbean and Central America between 1979 and 2018. Although analyzing the dynamical causes of only three dry intervals might not be enough to establish the ultimate cause of drought in our domain, our results provide further insights into the dynamics underpinning El Niño droughts in the Caribbean. Our results indicate that during these droughts anomalously large moisture divergence over the Caribbean Sea and Central America contrasts with above normal moisture convergence in the tropical Pacific. This is consistent with anomalous rising air over the eastern tropical Pacific, and subsidence over the

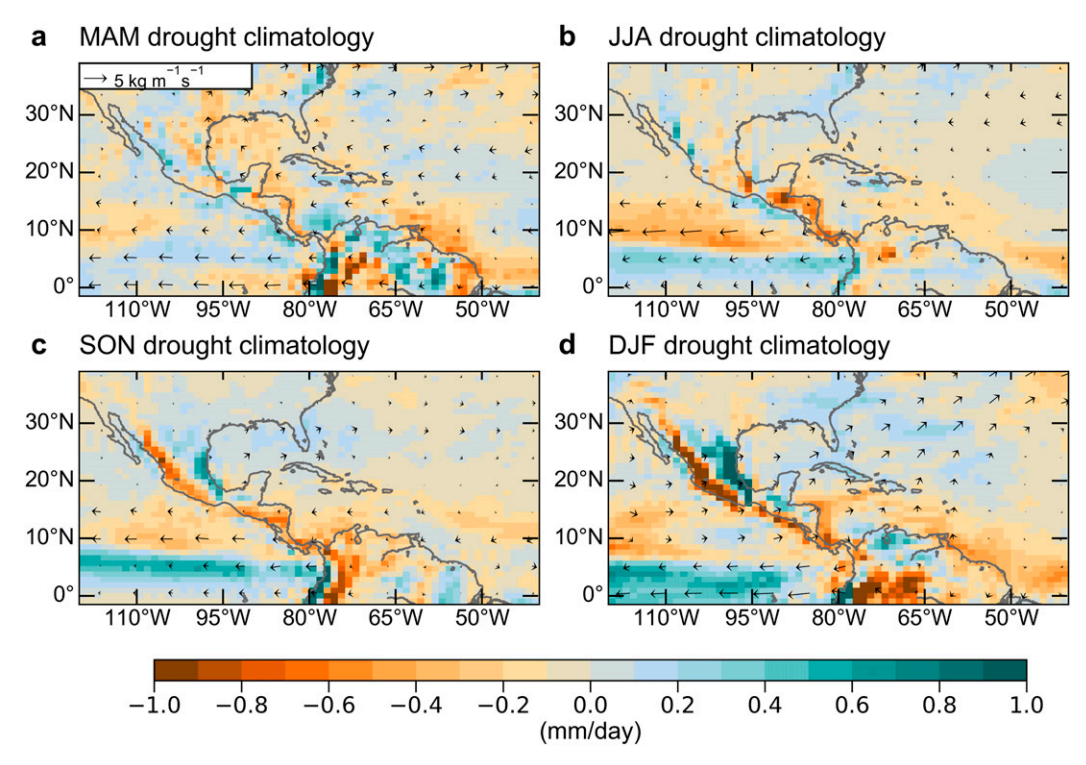


FIG. 21. As in Fig. 20, but for mass convergence anomalies. Notice the strong mass convergence over the eastern equatorial Pacific during JJA and SON, consistent with El Niño events from observations.

Caribbean Sea and northeastern South America. Also, we find that based on the droughts analyzed in this work, mass convergence is the main dynamical driver of drought in the Caribbean. In terms of SST anomalies, we find the typical

seesaw pattern between the tropical Pacific and tropical North Atlantic oceans, confirming the oceanic teleconnections described in previous work during El Niño (e.g., Giannini et al. 2000, 2001a,b).

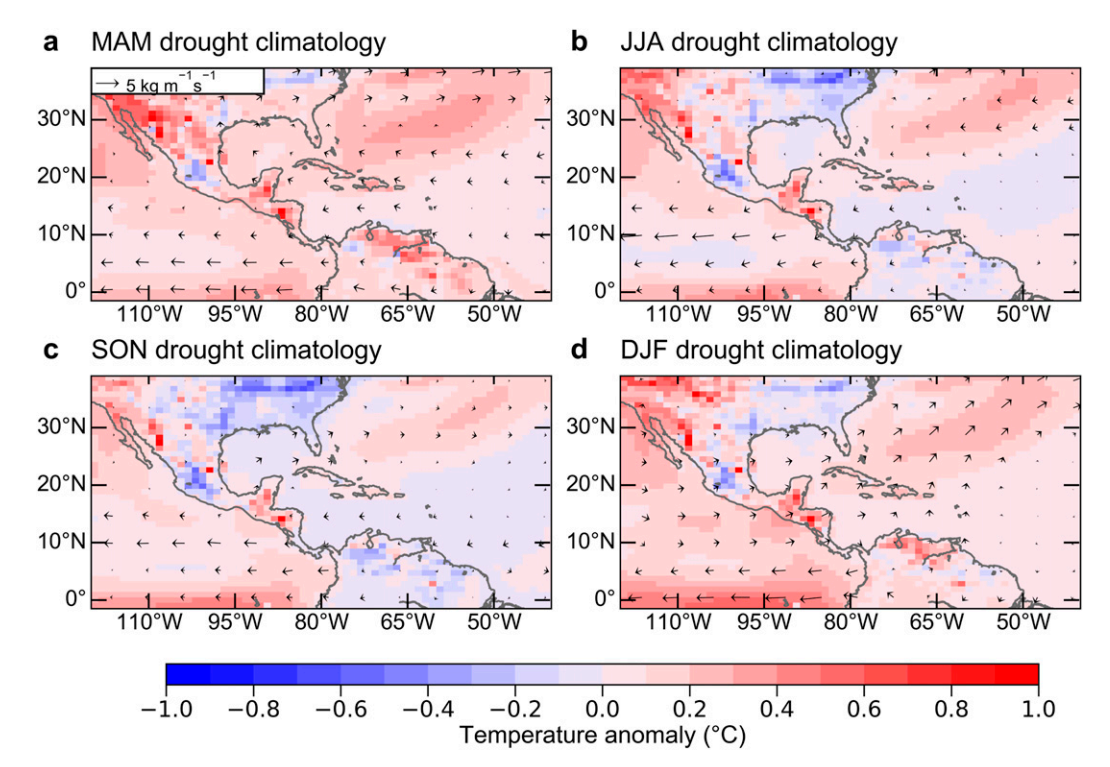


FIG. 22. Seasonal skin temperature anomalies during drought in LENS.

We also find that in general, CESM-LENS simulates well the dynamics underpinning drought in the Caribbean and Central America. Although biases in the magnitude of P - E and moisture flux anomalies exist, the geographic characteristics of these variables are similar to those observed in ERA-Interim. Furthermore, LENS shows droughts associated with a warmer than normal tropical Pacific, which is consistent with El Niño events. At least from the results with the 30-member ensemble we use in this work, LENS might be appropriate as a reference to evaluate the dynamics underpinning drought in the Caribbean and Central America. However, a more comprehensive assessment should be conducted using the 40 members of LENS, as well as a comparison with other climate models before using this model to evaluate changes in the dynamic origin of the Caribbean and Central America drying in response to climate change.

Acknowledgments. This material is partially supported by the National Science Foundation (NSF) EaSM2 Grant AGS-1243125, and NSF Grant AGS-1602564. This work is also supported by the National Center for Atmospheric Research (NCAR), which is a major facility sponsored by the NSF under the Cooperative Agreement 1852977. The efforts of Dr. Fasullo in this work were partially supported by the Regional and Global Model Analysis (RGMA) component of the Earth and Environmental System Modeling Program of the U.S. Department of Energy's Office of Biological and Environmental Research (BET) via NSF IA1844590. The European Centre for Medium-Range Weather Forecasts ERA-Interim reanalysis data were retrieved through the Research Data Archive at the NCAR, Computational and Information Systems Laboratory (https://doi.org/10.5065/P8GT-0R61, accessed 11 October 2019). We also thank Dr. Alessandra Giannini and the reviewers for their valuable comments and feedback to improve this work.

REFERENCES

- Adler, R. F., and Coauthors, 2003: The version-2 Global Precipitation Climatology Project (GPCP) monthly precipitation analysis (1979–present). J. Hydrometeor., 4, 1147–1167, https://doi.org/ 10.1175/1525-7541(2003)004<1147:TVGPCP>2.0.CO;2.
- Amador, J. A., 1998: A climatic feature of the tropical Americas: The trade wind easterly jet. *Top. Meteor. Oceanogr.*, **5**, 91–102.
- Anderson, T. G., K. J. Anchukaitis, D. Pons, and M. Taylor, 2019: Multiscale trends and precipitation extremes in the Central American midsummer drought. *Environ. Res. Lett.*, 14, 124016, https://doi.org/10.1088/1748-9326/ab5023.
- Ashok, K., S. K. Behera, S. A. Rao, H. Weng, and T. Yamagata, 2007: El Niño Modoki and its possible teleconnection. *J. Geophys. Res.*, **112**, C11007, https://doi.org/10.1029/2006JC003798.
- Bishop, D. A., and Coauthors, 2019: Investigating the causes of increased twentieth-century fall precipitation over the south-

- eastern United States. *J. Climate*, **32**, 575–590, https://doi.org/10.1175/JCLI-D-18-0244.1.
- Capotondi, A., and Coauthors, 2015: Understanding ENSO diversity. Bull. Amer. Meteor. Soc., 96, 921–938, https://doi.org/10.1175/BAMS-D-13-00117.1.
- Centella, A., A. Bezanilla, and K. Leslie, 2008: A study of the uncertainty in future Caribbean climate using the PRECIS regional climate model. Community Caribbean Climate Change Center Tech. Rep., 16 pp.
- Dee, D. P., and Coauthors, 2011: The ERA-Interim reanalysis: Configuration and performance of the data assimilation system. *Quart. J. Roy. Meteor. Soc.*, **137**, 553–597, https://doi.org/10.1002/qj.828.
- Durán-Quesada, A. M., L. Gimeno, and J. Amador, 2017: Role of moisture transport for Central American precipitation. *Earth Syst. Dyn.*, 8, 147–161, https://doi.org/10.5194/esd-8-147-2017.
- Enfield, D. B., and E. J. Alfaro, 1999: The dependence of Caribbean rainfall on the interaction of the tropical Atlantic and Pacific Oceans. *J. Climate*, **12**, 2093–2103, https://doi.org/10.1175/1520-0442(1999)012<2093:TDOCRO>2.0.CO;2.
- FAO, 2016: Situation report: Dry corridor in Central America. Food and Agriculture Organization of the United Nations, 3 pp., http://www.fao.org/-emergencies/resources/documents/resources-detail/en/c/422097/.
- Fasullo, J. T., and P. J. Webster, 2002: Hydrological signatures relating the Asian summer monsoon and ENSO. *J. Climate*, **15**, 3082–3095, https://doi.org/10.1175/1520-0442(2002)015<3082: HSRTAS>2.0.CO;2.
- Gamble, D. W., and S. Curtis, 2008: Caribbean precipitation: Review, model and prospect. *Prog. Phys. Geogr.*, 32, 265–276, https://doi.org/10.1177/0309133308096027.
- Giannini, A., Y. Kushnir, and M. Cane, 2000: Interannual variability of Caribbean rainfall, ENSO, and the Atlantic Ocean. J. Climate, 13, 297–311, https://doi.org/10.1175/1520-0442(2000) 013<0297:ivocre>2.0.co;2.
- —, M. A. Cane, and Y. Kushnir, 2001a: Interdecadal changes in the ENSO teleconnection to the Caribbean region and the North Atlantic Oscillation. J. Climate, 14, 2867–2879, https://doi.org/ 10.1175/1520-0442(2001)014<2867:ICITET>2.0.CO;2.
- —, J. C. Chiang, M. A. Cane, Y. Kushnir, and R. Seager, 2001b: The ENSO teleconnection to the tropical Atlantic Ocean: Contributions of the remote and local SSTs to rainfall variability in the tropical Americas. *J. Climate*, 14, 4530–4544, https://doi.org/ 10.1175/1520-0442(2001)014<4530:TETTTT>2.0.CO;2.
- Hernández Ayala, J. J., and M. Heslar, 2019: Examining the spatiotemporal characteristics of droughts in the Caribbean using the standardized precipitation index (SPI). Climate Res., 78, 103–116, https://doi.org/10.3354/cr01562.
- Herrera, D., and T. R. Ault, 2017: Insights from a new high-resolution drought atlas for the Caribbean spanning 1950–2016. J. Climate, 30, 7801–7825, https://doi.org/10.1175/JCLI-D-16-0838.1.
- —, —, J. T. Fasullo, S. J. Coats, C. M. Carrillo, B. I. Cook, and A. P. Williams, 2018: Exacerbation of the 2013–2016 Pan-Caribbean drought by anthropogenic warming. *Geophys. Res. Lett.*, **45**, 10 619–10 626, https://doi.org/10.1029/2018gl079408.
- Hidalgo, H. G., A. M. Durán-Quesada, J. A. Amador, and E. J. Alfaro, 2015: The Caribbean low-level jet, the inter-tropical convergence zone and precipitation patterns in the Intra-Americas Sea: A proposed dynamical mechanism. *Geogr. Ann.*, 97A, 41–59, https://doi.org/10.1111/geoa.12085.
- ——, E. J. Alfaro, J. A. Amador, and A. Bastidas, 2019: Precursors of quasi-decadal dry spells in the Central America dry corridor.

- Climate Dyn., **53**, 1307–1322, https://doi.org/10.1007/s00382-019-04638-y.
- Huang, B., and Coauthors, 2017: Extended Reconstructed Sea Surface Temperature version 5 (ERSSTv5), upgrades, validations, and intercomparisons. *J. Climate*, 30, 8179–8205, https://doi.org/10.1175/JCLI-D-16-0836.1.
- IPCC, 2014: Climate Change 2014: Synthesis Report. R. K. Pachauri and L. A. Meyer, Eds., IPCC, 151 pp.
- Jury, M., B. A. Malmgren, and A. Winter, 2007: Subregional precipitation climate of the Caribbean and relationships with ENSO and NAO. J. Geophys. Res., 112, D16107, https://doi.org/10.1029/2006JD007541.
- Karnauskas, K. B., J. P. Donnelly, and K. J. Anchukaitis, 2016: Future freshwater stress for island populations. *Nat. Climate Change*, 6, 720–725, https://doi.org/10.1038/nclimate2987.
- —, C. F. Schleussner, J. P. Donelly, and K. J. Anchukaitis, 2018: Freshwater stress on small island developing states: Population projections and aridity changes at 1.5 and 2°C. Reg. Environ. Change, 18, 2273–2282, https://doi.org/10.1007/s10113-018-1331-9.
- Kay, J. E., and Coauthors, 2015: The Community Earth System Model (CESM) large ensemble project: A community resource for studying climate change in the presence of internal climate variability. *Bull. Amer. Meteor. Soc.*, 96, 1333–1349, https://doi.org/10.1175/BAMS-D-13-00255.1.
- Larsen, M. C., 2000: Analysis of 20th century rainfall and streamflow to characterize drought and water resources in Puerto Rico. *Phys. Geogr.*, 21, 494–521, https://doi.org/10.1080/02723646. 2000.10642723.
- Magaña, V., J. A. Amador, and S. Medina, 1999: The midsummer drought over Mexico and Central America. *J. Climate*, 12, 1577–1588, https://doi.org/10.1175/1520-0442(1999)012<1577: TMDOMA>2.0.CO:2.
- Martin, E. R., and C. Schumacher, 2011: Modulation of Caribbean precipitation by the Madden–Julian oscillation. *J. Climate*, 24, 813–824, https://doi.org/10.1175/2010JCLI3773.1.
- Martinez, C., L. Goddard, Y. Kushnir, and M. Ting, 2019: Seasonal climatology and dynamical mechanisms of rainfall in the Caribbean. *Climate Dyn.*, 53, 825–846, https://doi.org/10.1007/ s00382-019-04616-4.
- Méndez, M., and V. Magaña, 2010: Regional aspects of prolonged meteorological droughts over Mexico and Central America. J. Climate, 23, 1175–1188, https://doi.org/10.1175/2009JCLI3080.1.
- Neelin, J. D., H. Münnich, H. Su, J. E. Meyerson, and C. E. Holloway, 2006: Tropical drying trends in global warming models and observations. *Proc. Natl. Acad. Sci. USA*, 103, 6110–6115, https://doi.org/10.1073/pnas.0601798103.
- OCHA, 2015: Drought in Central America in 2015: Situation report (as of October 6, 2015). United Nations Office for the Coordination of Humanitarian Affairs (OCHA), 5 pp., https://reliefweb.int/report/guatemala/drought-central-america-2015-situation-report-october-6-2015.
- Peters, E. J., 2015: The 2009/2010 Caribbean drought: A case study. *Disasters*, 39, 738–761, https://doi.org/10.1111/disa.12123.
- Rauscher, S. A., F. Giorgi, N. S. Diffenbaugh, and A. Seth, 2008: Extension and intensification of the Meso-American midsummer drought in the twenty-first century. *Climate Dyn.*, 31, 551–571, https://doi.org/10.1007/s00382-007-0359-1.

- Rogers, J. C., 1988: Precipitation variability over the Caribbean and tropical Americas associated with the Southern Oscillation. *J. Climate*, **1**, 172–182, https://doi.org/10.1175/1520-0442(1988) 001<0172:PVOTCA>2.0.CO;2.
- Schneider, U., A. Becker, P. Finger, A. Meyer-Christoffer, B. Rudolf, and M. Ziese, 2015a: GPCC full data reanalysis version 7.0 at 1.08: Monthly land-surface precipitation from raingauges built on GTS-based and historic data. Global Precipitation Climatology Centre, accessed October 2019, https://doi.org/ 10.5676/DWD_GPCC/FD_M_V7_100.
- —, —, —, and M. Ziese, 2015b: GPCC monitoring product: Near real-time monthly land-surface precipitation from rain-gauges based on SYNOP and CLIMAT data. Global Precipitation Climatology Centre, accessed October 2019, https://doi.org/10.5676/DWD_GPCC/MP_M_V5_100.
- Seager, R., and N. Henderson, 2013: Diagnostic computation of moisture budgets in ERA-Interim reanalysis with reference of analysis of CMIP-archived atmospheric model data. *J. Climate*, 26, 7876–7901, https://doi.org/10.1175/JCLI-D-13-00018.1.
- —, L. Goddard, J. Nakamura, N. Henderson, and D. E. Lee, 2014: Dynamical causes of the 2010/11 Texas–northern Mexico drought. *J. Hydrometeor.*, **15**, 39–68, https://doi.org/10.1175/JHM-D-13-024.1.
- Taylor, M. A., D. B. Enfield, and A. A. Chen, 2002: Influence of the tropical Atlantic versus the tropical Pacific on Caribbean rainfall. J. Geophys. Res., 107, 3127, https://doi.org/10.1029/2001JC001097.
- —, F. S. Whyte, T. S. Stephenson, and J. D. Campbell, 2013: Why dry? Investigating the future evolution of the Caribbean low-level jet to explain the projected Caribbean dying. *Int. J. Climatol.*, **33**, 784–792, https://doi.org/10.1002/joc.3461.
- Torres-Valcárcel, A. R., 2018: Teleconnections between ENSO and rainfall and drought in Puerto Rico. *Int. J. Climatol.*, **38**, e1190–e1204, https://doi.org/10.1002/joc.5444.
- Trenberth, K. E., 1991: Climate diagnostics from global analyses: Conservation of mass in ECMWF analyses. *J. Climate*, **4**, 707–722, https://doi.org/10.1175/1520-0442(1991)004<0707:CDFGAC>2.0. CO:2.
- —, and C. J. Guillemot, 1996: Physical processes involved in the 1988 drought and 1993 floods in North America. *J. Climate*, 9, 1288–1298, https://doi.org/10.1175/1520-0442(1996)009<1288: PPHTD>2.0.CO;2.
- —, and J. T. Fasullo, 2018: Applications of an updated atmospheric energetics formulation. *J. Climate*, 31, 6263–6279, https://doi.org/10.1175/JCLI-D-17-0838.1.
- —, J. W. Hurrell, and A. Solomon, 1995: Conservation of mass in three dimensions in global analyses. *J. Climate*, **8**, 692–708, https://doi.org/10.1175/1520-0442(1995)008<0692;COMITD>2.0. CO:2.
- —, J. T. Fasullo, and J. Mackaro, 2011: Atmospheric moisture transports from ocean to land and global energy flows in reanalyses.
 J. Climate, 24, 4907–4924, https://doi.org/10.1175/2011JCLI4171.1.
- Williams, A. P., B. I. Cook, J. E. Smerdon, D. A. Bishop, R. Seager, and J. Mankin, 2017: The 2016 southeastern U.S. drought: An extreme departure from centennial wetting and cooling. *J. Geophys. Res.* Atmos., 122, 10 888–10 905, https://doi.org/10.1002/2017jd027523.